GROWTH OF CARBON NANOTUBES AND SEMICONDUCTOR NANOWIRES ON SILICON BY CHEMICAL VAPOR DEPOSITION

By

KI-HONG LEE

A DISSERTATION PRESENTED TO THE GRADUATE SCHOOL
OF THE UNIVERSITY OF FLORIDA IN PARTIAL FULFILLMENT
OF THE REQUIREMENTS FOR THE DEGREE OF
DOCTOR OF PHILOSOPHY

UNIVERSITY OF FLORIDA

2004

This document is dedicated to my father.

ACKNOWLEDGMENTS

Above all, I am tremendously grateful to Dr. Wolfgang Sigmund, my supervisory committee chair. He provided sincere guidance and support for 4 years. It is also my great honor to have four other professors (Dr. David Norton, Dr. Susan Sinnott, Dr. Rajiv Singh, and Dr. Andrew Rinzler) as my committee members.

For the characterization of samples, I thank Kerry Siebein and Micheal Tollen of the Major Analytical Instrument Center (MAIC) for high resolution transmission electron microscopy (HRTEM) and field emission scanning electron microscopy (FESEM) analysis. I would like thank to Dr. Won-Seon Seo, Dr. Yongho Lee, Dr. Myung-Hyun Lee of the Korea Institute of Ceramic Engineering and Technology (KICET) for HRTEM analysis, and Dr. Richard Vanfleet of the Advanced Materials Processing and Analysis Center (AMPAC).

I also appreciate the valuable help of my colleagues in Dr. Sigmund's group. In particular, I thank Hansoo Kim, Jeong-Min Cho, and Seung-Woo Lee for SEM and TEM work. Finally, I deeply and sincerely appreciate the encouragement and support of my mother and brothers.

TABLE OF CONTENTS

page

LIST OF TABLES

LIST OF FIGURES

Abstract of Dissertation Presented to the Graduate School
of the University of Florida in Partial Fulfillment of the
Requirements for the Degree of Doctor of Philosophy

GROWTH OF CARBON NANOTUBES AND SEMICONDUCTOR NANOWIRES ON SI BY CHEMICAL VAPOR DEPOSITION

By

Ki-Hong Lee

May 2004

Chair: Wolfgang M. Sigmund
Major Department: Materials Science and Engineering

Carbon nanotubes (CNTs) are a promising material for nano-electronic devices because of their electrical properties and very small diameter. However, controlling their electronic properties depending on chirality and tube diameter of the CNTs and growth direction of the CNTs has been a challenge for realizing nanotube-based electronic devices. Until now, the growth mechanism of CNTs was not fully understood and controlling the growth of CNTs completely is still a major challenge. Understanding of the growth mechanism of CNTs is an essential in order to achieve controllability in both growth direction and electrical properties of nanotubes by chemical vapor deposition (CVD). There are many variables, however, to consider in this process, including the type of gases, catalyst metals, and supporting substrates.

Supporting substrates of the catalyst metals are also an important factor in the growth of carbon nanotube. It is known that interaction between catalyst particle and support is required for catalytic activity. In particular, oxygen-containing materials are

known as a suitable support for this purpose. Our study is focused on the growth mechanism of CNTs on silicon oxide by chemical vapor deposition (CVD). In particular, the chemical interaction between the vapor phase and the supporting oxide is investigated relating to the growth mechanism of CNTs.

Methane (CH_4) and hydrogen (H_2) are used as reaction gases and nickel is used as a catalyst. CO is generated by chemical interaction between the supporting oxide and the process gases; thereby complicates the composition of the gas components in CVD process. In order to modulate CO vapor concentration in the system, metal oxide powders, such as titanium oxide (TiO_2), silicon oxide (SiO_2) and silicon oxide/iron nitrate mixture are adopted based on the thermodynamic calculation of CO vapor pressure of the each oxide in the CH_4-H_2 system.

Nanotubes can be used individually or as an ensemble to build a functional device prototype. Ensembles of nanotubes have been used for field emission based flat panel display. Individual nanotubes have been used for field emission sources and as tips for scanning probes. Nanotubes also have significant potential as the central elements of nano-electronic devices including field effect transistors (FETs), single-electron transistors, and rectifying diodes. In an effort to find a way to align carbon nanotubes on silicon substrate, the growth orientation of carbon nanotube is investigated on single crystal iron nano particles on silicon wafer. The iron nano particles are adhered to the substrate by magnetic field from dispersion. Our study suggests the possibility of controlling the growth orientation of the CNTs. Furthermore, novel evidence is given for the growth mechanism of the CNTs by CVD.

CHAPTER 1
INTRODUCTION

Since Iijima[1] discovered the carbon nanotubes (CNTs), many research groups have studied their synthesis,[2,3] mechanical properties,[4]and electrical properties.[5,6,7] A single-walled carbon nanotube (SWNT) can be either metallic or semiconducting, depending on diameter and chirality of the nanotubes.[8,9] The small size of a CNT makes it a potential candidate for nano-electronic devices.

Nanotubes can be used individually or as an ensemble to build a functional device prototype. Ensembles of nanotubes have been used for field emission based flat panel display. Individual nanotubes have been used for field emission sources and tips for scanning probes. Nanotubes also have significant potential as the central elements of nano-electronic devices including field effect transistors (FETs), single-electron transistors and rectifying diodes. Several research groups showed that field effect transistors (FETs) using semiconducting nanotubes as a channel operate successfully at room temperature.[10] Collins et al.[9] reported a method that tailors the electrical properties of carbon nanotubes by using electrical breakdown. However, they produced FETs circuit one at a time, and with much effort by attaching a nanotube to metal electrodes. Thus, this approach is not suitable for producing microchips.

Even though many research groups have reported the feasibility of CNTs for nano-electronic devices, there are critical problems to be solved for its integration into devices. One problem is how to produce carbon nanotubes with unified electrical properties on a substrate. To grow CNTs with specific electrical properties are needed for each device.

However, electrical properties of nanotubes vary according to diameter and chirality, making it difficult to produce CNTs with common characteristics. The other problem is how to control the growth direction of CNTs. For the emitter and the contact material, CNTs must be aligned vertically; and for the channel, CNTs must be aligned laterally on a substrate. Vertically aligned CNTs have been produced by using chemical vapor deposition (CVD) over catalyst particles patterned on a porous substrate,[11] and on a glass substrate by plasma enhanced CVD.[12]

In contrast to vertical growth, lateral growth of CNTs has received little attention because of its difficulty. Lateral growth of CNTs is less likely to be achieved experimentally, and the possibility of lateral growth of CNTs has not been proven yet. Even though the growth mechanism is not fully understood, vertically aligned CNTs in patterned arrays have been produced using various types of CVD. There have been few reports, however, on the lateral growth of CNTs. Dai et al.[13,14] showed the possibility that CNTs could be produced parallel to the substrate by using suspended catalysts made by a lift-off process. They attributed parallel growth of nanotubes to reaction gas flow. One other research group[15] reported CNTs grown parallel to substrates by using an oxide layer to suppress vertical growth of the CNTs. Until now, however, no successful method has been suggested for laterally aligning CNTs on the substrate surface. As a matter of fact, realization of integrated nanotube transistors depends on whether laterally aligned CNTs can be produced on Si substrate.

Recent interest in CVD nanotube growth is also due to the idea that aligned and ordered nanotubes structure can be grown on substrates, such as Si, with control that is not possible with arc-discharge or laser ablation techniques. [16] Furthermore, the growth

location of the nanotube is precisely determined by the location of the catalyst on the substrate.[17] Vertically aligned carbon nanotubes have been produced successfully by several research groups. Multi-walled nanotubes (MWNTs) can self-assemble into aligned structures as they grow, and the driving force for self-alignment is the Van der Waals interaction between nanotubes.[18] During CVD growth, the outermost walls of nanotubes interact with their neighbors (via Van der Waals forces) to form a rigid bundle, which allows the nanotubes to grow perpendicular to the substrate. Recently, by patterning metal catalyst, uniform arrays of nanotubes and single free-standing aligned nanotubes at precise locations were reported.[19]

An understanding of the growth mechanism of CNTs is needed to achieve controllability in both growth direction and electrical properties of nanotubes by CVD. There are many variables, however, to consider in this process, including the type of gases, catalyst metals, and supporting substrates. Several kinds of gases are necessary for the synthesis of CNT by CVD. Hydrocarbon gases, such as methane (CH_4), ethane (CH_2), acetylene (C_2H_2), and carbon monoxide (CO) are usually used for the carbon source by CVD. Ammonia (NH_3) and hydrogen (H_2) are used for pre annealing and controlling decomposition kinetics of the carbon source gases. Transition metals, such as iron (Fe), cobalt (Co), and nickel (Ni), are normally used as a catalyst for the synthesis of CNT by CVD. Catalytic metals play an important role for CNT growth as a carbon generation source and as a medium for the nucleation of CNTs. The formation of these nanotubes mats results from a sorption/solid solution/precipitation process in the small metal particles. Carbon diffuses to the metal particles, is absorbed, diffuses through the particle, and finally precipitates as a CNT on the growth surface of the particle. The growth

behavior of CNT is a complicated process (depending on the type of carbon source gas, gas composition, growth temperature, catalyst metals and supporting substrate). Therefore, there are controversial issues regarding the catalytic efficiency of the metals.

Supporting substrates of the catalyst metals are also an important factor in the growth of carbon nanotube. It is well known that interaction between catalyst particle and support is required for catalytic activity. In particular, oxygen-containing materials are known as a suitable support for this purpose. Although many reports exist on the type and quality of oxide materials for CNT growth, the effect of supporting oxides remains unclear. Until now, studies on the relationship between catalyst metals and supporting oxides have focused on catalytic efficiency. However, the challenge is to define a unified growth mechanism for CNTs that can be applied to every experimental condition. In addition, experimental conditions for CNT growth are very similar to the ones for silicon those for carbide and silica nanowire growth.

Until now, there has been little interest in the chemical species created by the supporting oxide and their impacts on the growth mechanism of CNTs. In our study, the chemical interaction between the vapor phase and the supporting oxide is investigated relating to the growth mechanism of CNTs. In addition, the correlation between a synthesized nano phase (including CNTs, SiC and SiO_2 nanowire) and a gas composition change is discussed. Thermodynamic and chemical reactions in the growth system are investigated in an effort to explore the growth mechanism of the synthesized nanostructures on the substrates. Synthesis temperature (1050°C), input gases (CH_4:H_2), and supporting oxide (thermally grown silica on Si substrate) are fixed to investigate the growth characteristics of CNTs. To create a controlled gas species in the system, metallic

or oxide powders such as titanium (Ti), titania (TiO_2) and silica (SiO_2) are incorporated in the growth system. In addition to that, the possibility of controlling the growth orientation of the CNTs is discussed for the potential application of CNTs in nano-electronic devices. Novel evidence is given for the growth mechanism of the CNTs.

CHAPTER 2
LITERATURE REVIEW

2.1 Structure of Carbon Nanotubes

Carbon nanotubes are grown by the diffusion of carbon via catalytic decomposition of carbon containing gases or vaporized carbon from arc discharge or laser ablation. Carbon nanotubes are normally classified into two types; single wall and multi wall. The multi wall carbon nanotube contains several concentric and coaxial graphene cylinders. The intershell spacing can range from 0.34 to 0.39 nm.[20-22] Each shell in multi wall carbon nanotubes is uncorrelated to each other in terms of structure and properties. For example, if a multi wall carbon nanotube is contacted on the outside, the electric current is conducted through its outermost shell only.[23]

The structure of carbon nanotubes is essentially graphitic. Carbon nanotubes behave like rolled-up cylinders of graphene sheets of sp^2 bonded carbon atoms. Generally we specify carbon nanotubes in terms of the tube diameter d_t, and the chiral angle θ, which are shown in Fig. 2-1.[24] Armchair nanotubes are formed when $n = m$ and the chiral angle is 30°. Zigzag nanotubes are formed when either n or m is zero and the chiral angle is 0°. All other nanotubes with chiral angles intermediate between 0° and 30° are known as chiral nanotubes. Figure 2-2 shows a 3-dimensional nanotube structure for each case.

The properties of nanotubes are determined by their diameter and chiral angle, both of which depend on n and m. The diameter, d_t, is simply the length of the chiral vector divided by ¼, and we find that $d_t = 3^{1/2} a_{c\text{-}c} (n^2 + nm + m^2)^{1/2}/\pi$, where $a_{c\text{-}c}$ is the

distance between neighboring carbon atoms in the flat sheet. In turn, the chiral angle is given by $\tan^{-1}(3^{1/2}n/(2m + n))$. Measurements of the nanotube diameter and the chiral angle have been made with scanning tunnelling microscopy and transmission electron microscopy.

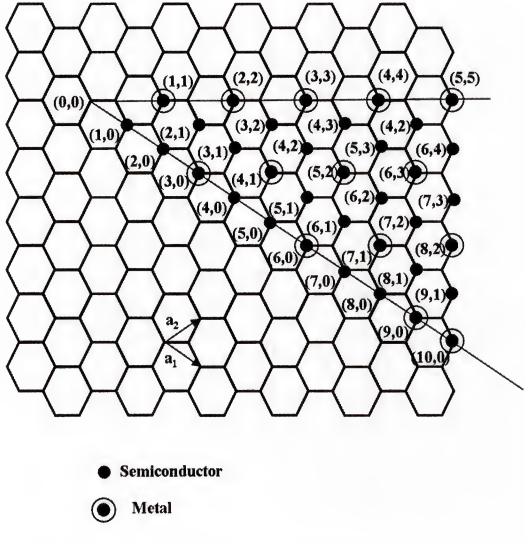

Figure 2-1. The 2D graphene sheet is shown along with the vector that specifies the chiral nanotube. The chiral vector $Ch = na_1 + ma_2$ is defined on the honeycomb lattice by unit vectors a_1 and a_2 and the chiral angle θ is defined with respect to the zigzag axis. Along the zigzag axis $\theta = 0°$. The diagram is constructed for (n,m) = (6,2). dt (diameter) = $|Ch|/\pi = a(n2+m2+nm)^{1/2}/\pi$, $\tan\theta = 3^{1/2}m/(2n + m)$. a: length of unit vector a_1 and a_2.

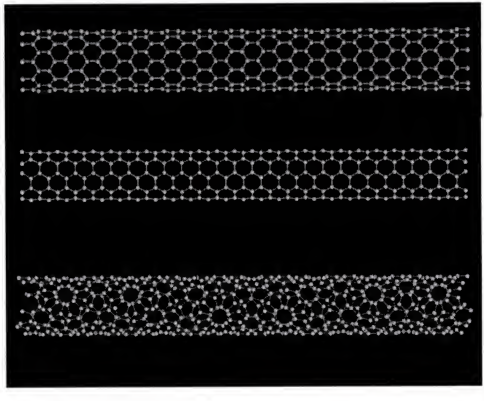

Figure 2-2. By rolling up a graphene sheet (a single layer of carbon atoms from a 3D graphite crystal) as a cylinder and capping each end of the cylinder with half of a fullerene molecule, a "fullerene-derived tubule," one layer in thickness, is formed. Shown here is a schematic theoretical model for a single-wall carbon tubule with the tubule axis normal to: (a) the $\theta = 0°$ direction (an "zigzag" tubule), (b) the $\theta = 30°$ direction (a "armchair" tubule), and (c) a general direction B with $0 < \theta < 30°$ (a "chiral" tubule). The actual tubules shown in the figure correspond to *(n,m)* values of (a) (10,0), (b) (5,5), and (c) (8,3).

The unique electronic properties of carbon nanotubes are due to the quantum confinement of electrons normal to the nanotube axis. Observation of one dimensional quantum effects in carbon nanotubes requires tubes of sufficiently small diameter in the range of $1 \sim 20$ nm, depending on the properties under investigation.[24,25] In the radial direction, electrons are confined by the monolayer thickness of the graphene sheet. In general, a (n, m) carbon nanotube will be metallic when $n - m = 3q$, where q is an integer. All armchair nanotubes are metallic, as are one-third of all possible zigzag nanotubes.

Figure 2-3 shows electrical properties of carbon nanotubes depending on the diameter and the chirality.

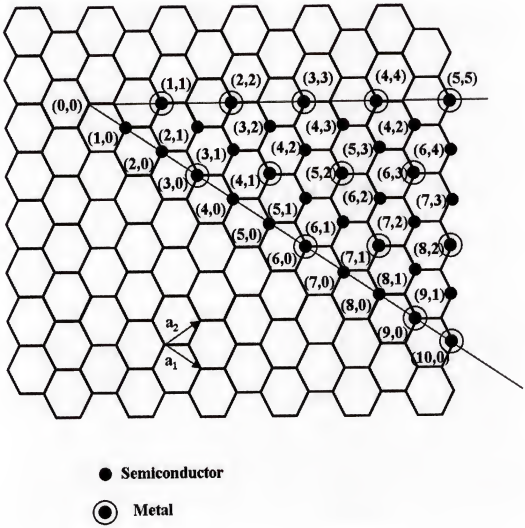

Figure 2-3. The 2D graphene sheet is shown along with the vector, which specifies the chiral nanotube. The pairs of integers (n,m) in the figure specify chiral vectors C_h, (See figure 2-1) for carbon nanotubes, including zigzag, armchair, and chiral tubules. Below each pair of integers (n,m) is listed the number of distinct caps that can be joined continuously to the cylindrical carbon tubule denoted by (n, m). The circled dots denote metallic tubules and the small dots are for semiconducting.

As shown in Fig. 2-3, single wall carbon nanotubes can be metallic or semiconducting (typically 0.4 ~ 0.7 eV bandgap) depending on the orientation of hexagons with respect to the diameter (chirality). Among the carbon nanotubes that are

semiconducting, their band gap is inversely proportional to their diameter, independent of the tube chirality. [26,27] In the case of a multi-wall carbon nanotube, conduction occurs through the outermost shell. As a result, the large diameter of the outer nanotube causes the nanotube to be metallic.

2.2. Synthesis of Carbon Nanotubes by Catalytic CVD

2.2.1. Growth Mechanism of Carbon Nanotube by Catalytic CVD

The catalytic synthesis of CNTs normally occurs in flowing gaseous components containing a certain proportion of hydrocarbon such as CH_4, C_2H_4 and C_2H_2 mixed with H_2 or CO over small transition metal particles. Many parameters (including the temperature, gas composition, and catalyst nature and size) affect the nature of the resulting carbon products.

Baker et al.[28] showed that the linear filament growth rate varies inversely with the radius of the catalytic particles. They proposed a growth mechanism for CNT as a succession of the following processes: (1) gas adsorption at the catalyst metal surface, (2) creation of a source of carbon atoms by the decomposition process by the catalyst metals, (3) dissolution in and diffusion of carbon atoms through the metal particles, (4) re-precipitation of the carbon species to form nanotube structure. [29,30] Since the energy of the (0001) basal plane of graphite is exceptionally low, it is energetically favorable for the CNT to grow with the basal planes to minimize lattice mismatch with the metal crystallographic orientation. The crystallographic arrangement of the metal particles will determine the growth direction of the CNT.

Another research group [31] proposed a growth model related to the surface diffusion of carbon species on the catalyst particle, which is "liquid like". The carbon will eventually dissociate at the contact angle between the particle and the substrate, thereby

precipitate to produce carbon shell structures. The growth mechanism proposed by Tibbetts[3] is that molecular decomposition and carbon dissolution occur at one side of a catalytic particle. The consequent gradient in chemical potential causes bulk diffusion of carbon to the back face of the particle where a carbon shell begins to form. Technically, there is little difference between the growth mechanisms. All mechanisms follow a similar procedure: 1) dissolution of carbon in the catalyst metal; 2) diffusion to a certain part and 3) re-precipitation of carbon. Baker's and Oberlin's models[28-31] are shown in Figure 2-4.

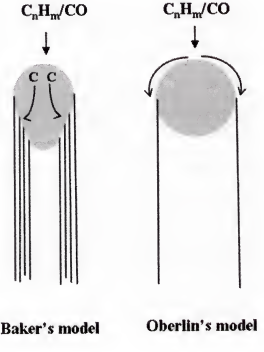

Figure 2-4. The growth model of carbon nanotubes by Baker and Oberlin.

A model for the formation of cylindrical layers around a hollow core was suggested by Tibbetts.[3] The creation of the new graphitic layers of the carbon nanotubes leads to a change in the chemical potential associated with condensation of the carbon from the gaseous phase. The change in the chemical potential to form the cylindrical shell of

length *dl*, with the outer radius of r_o and the inner radius of r_i is given in Equation 2-1:[3,32,33]

$$\Delta\mu = \Delta\mu_0 - (\Delta E_{surface}/dn) - (\Delta E_{strain}/dn)$$
$$\Delta\mu = -\delta G/dn; \qquad dn = dV/\Omega = \pi(r_o^2 - r_i^2)dl/\Omega \qquad (2\text{-}1)$$
$$\Delta E_{surface} = 2\pi(r_o - r_i)\sigma dl; \qquad \Delta E_{strain} = (\pi/12)\varepsilon(r_o - r_i)^2\ln(r_o/r_i)dl$$

δG: Gibbs free energy change; dV: volume change of a growing tube; dn: the change in the number of carbon atoms; Ω: volume occupied by a carbon atom in graphite; ε: Young's modulus for graphite; σ: unit area of the solid surface.

The critical radius of carbon nanotube can be calculated from the energy balance between the elastic energy stored in the bending of the graphite layer and the energy recovered from the stitching of its dangling bonds. The prediction of a minimum inner diameter ($r_i > 5$ nm) for a carbon fiber suggests that the Tibbetts model for vapor-grown carbon fibers cannot be extended to carbon nanotubes directly and that a new mechanism is needed for stabilizing the very small inner diameter of the carbon nanotubes ($r_i << 5$ nm). The new mechanism arises from the tubule cap, which is stable down to a diameter of $\cong$ 1 nm.[34]

2.2.2. Catalytic Synthesis of Carbon Nanotube in a Hydrocarbon-H_2 System

A few hydrocarbon gases are well known for the catalytic synthesis for CNTs. The growth temperature of the CNT is dependent on the type of hydrocarbon gas feed. And, the structure of the CNT depends mainly on growth temperature. Acetylene has been widely used for low temperature growth of CNTs. In addition, the catalytic decomposition rate is sufficiently high to allow formation of aligned carbon nanotube films[35,36] without the necessity of using template substrate materials. A disadvantage of the gas is its self-pyrolysis to produce unwanted amorphous carbon. Methane is the most prominent precusor for thermal CVD production of single wall carbon nanotube (SWNT).[37-39] The CNTs produced by CVD of methane are generally characterized by

high quality because of its low self-pyrolysis rate. Ethylene is positioned between methane and acetylene regarding its function as a CNT precusor.[40,41]

Hydrogen is a crucial component for the synthesis of CNT by CVD. The functions of hydrogen can be described as 1) reducing catalysts that might become partially oxidized in the absence of hydrogen and 2) controlling the decomposition rate for the hydrocarbon gases. For example, the equilibrium of the disproportionation reaction, $CH_4 \rightarrow C + 2H_2$, will shift to the left side as the hydrogen concentration increases, thereby limiting the non-catalytic decomposition of methane. Generally, for larger CH_4-H_2 ratios than the optimum ratio, the relative amount of non-tubular carbon increases.[42] However, hydrogen's impact on the catalyst and the role of atomic hydrogen remain as challenges.

2.2.3. Catalytic Synthesis of CNT by CO Disproportionation

Higher temperatures are desirable in order to anneal away defects that form in the growing nanotube. Since the rate of pyrolysis of the hydrocarbon feedstock overwhelms the rate of tube growth higher than 800 to 900°C, an undesirable amorphous overcoating forms above these temperatures. Carbon monoxide as a carbon source does not suffer from this problem, since it decomposes significantly in the vapor only at a much higher temperature.

Dai et al.[43] showed that CO can be used as a feedstock for SWNT using molybdenum (Mo) catalyst. They proposed a mechanism, called the yarmulke mechanism, wholly different from those for the catalytic formation of MWNTs.[3,28-31] Nano-sized metal particle has a very high surface energy, resulting in the formation of a graphene cap (the yarmulke) to decrease their total surface energy with its edges strongly chemisorbed to the metal. Since the basal plane of graphite has an extremely low surface

energy (10 to 20 times smaller than most metals), the total surface energy diminishes by forming the cap. Newly arriving carbon will continue to assemble on the surface of the catalyst in three ways: 1) the original cap can continue to grow around the particle, which results in the deactivation of the catalyst, 2) a second cap can form underneath and lift up the first, which will form a cylindrical tube, and 3) carbon can add to the cylindrical section of a growing layer.

Nikolaev et al.[44] synthesized SWNTs using a gas-phase catalyst, iron pentacarbonyl ($Fe(CO)_5$). The formation of SWNT from CO based on the Boudouard reaction

$$CO + CO \xrightarrow{Catalyst} C + CO_2 \qquad (2\text{-}2)$$

They performed an experiment in which a small amount of CH_4 was added to the CO flow to increase the amount of carbon available for SWNT growth. However, higher CH_4 concentration (>1.4%) resulted in the formation of an undesirable amorphous phase by self-pyrolysis of methane.

2.2.4. Carbon Nanotube Growth by PECVD

Plasma enhanced CVD (PECVD) has been investigated for its ability to produce vertically-aligned nanotubes. Even though there is enough empirical evidence that the electric field in the plasma enables more vertically aligned CNTs than thermal CVD[45-47] the true role of the plasma in CNT growth is not clear. Typical hydrocarbon sources used in plasma-based growth of CNTs include methane, ethylene, and acetylene. Since the plasma can dissociate the hydrocarbon, creating a lot of reactive radicals, the use of pure hydrocarbon feedstock may lead to substantial amorphous carbon deposition. Therefore, it is desirable to dilute the hydrocarbon with argon hydrogen, or ammonia.[45-49]

Bower performed experiments to investigate the alignment mechanism of the nanotubes using high-frequency, microwave PECVD.[50] They found that nanotube growth always occurs perpendicular to the local substrate surface regardless of the substrate tilt or shape. They suggested that the electrical self-bias imposed on the substrate surface appears to be the primary mechanism responsible for conformal alignment. Another research group claimed that anisotropic etching accounts for the vertical alignment of carbon nanotubes.[51] They suggested that nanotubes growing in random orientations were unprotected by their metal catalyst particles and hence were preferentially etched away in the plasma.

2.3. Important Parameters for the Synthesis of CNT by Catalytic CVD

2.3.1. Catalyst Supporting Materials

Supporting material for catalyst metals is an important parameter for the catalytic synthesis of carbon nanotube. Oxide materials, including silica, alumina and zeolite, are empirically known as a good support for the purpose. Generally, interaction between a catalyst and a support can be characterized in two aspects. Typically mentioned with regard to the interaction is the contact angle between the support and the catalyst. Nickel (Ni) on silica (SiO_2) has a large contact angle (which means a weak interaction between them) at high temperature, and thus the top growth is favored.[52] Cobalt (Co) or iron (Fe) on silicon favors the base growth. [50-53] In this case, however, the metals react with silicon to form a silicide phase at high temperature. Thus, the chemical interaction between the catalyst and its support should be considered.

In terms of efficiency of the catalyst, the support material should not react with the catalyst at the synthesis temperature. Several research groups[54,55] adopted a titanium (TiN) layer as a diffusion barrier to prevent reaction between the catalysts and silicon.

They suggested that using TiN as a barrier improves the nanotube yield on silicon substrates. However, the effect of support or barrier on the catalyst efficiency is still controversial. For example, Nerushev et al. [56] reported that carbon nanotube does not grow on Fe/Ti substrates using CH_4 at 1100°C. In contrast, it was also reported that multi wall carbon nanotubes can be synthesized on Fe/Ti substrates using C_2H_2 at 700 °C. [57]

The distinction between growth mechanisms, called the top growth and the bottom growth, seems not to be essential because in both cases the CNT grows away from the particle by the precipitation of carbon in the contact region between the particle and the tube segment.

2.3.2. Catalyst

The catalyst is usually prepared and applied to the substrate in some type of wet chemical, nanoparticle, and film. In the wet catalyst method, soluble salts such as iron nitrate ($Fe(NO_3)_3 \cdot 9H_2O$) and $Ni(NO_3)_2 \cdot 6H_2O$ are typically used.[58] The salt solution is normally reduced to oxide nanoparticles by heating. During synthesis, this oxide is reduced to metal nanoparticles and will catalyze the growth of carbon nanotubes. Actually, the effect of pre-reduction of oxide catalysts is unclear. Fonseca et al.[59] reported pre-reduction of cobalt oxide (CoO) on silica particles prepared by cobalt acetate ($Co(CH_3COO)_2$. They reported that hydrogenation has only disadvantageous effects on the performance of the catalysts. The catalyst solution is applied on the substrate using spin coating[60] or microcontact printing.[61]

Another very common and simple technique of depositing the metal catalyst is physical vapor deposition, such as sputtering and evaporation. When this catalyst film is heated to a high temperature, the film breaks up and forms metal clusters that catalyze the

growth of carbon nanotubes. The size of the metal clusters depends on the thickness of the catalyst films [62] and the annealing temperature. [63,64] However, the size of catalyst is not simply controlled by the parameters since the formation of clusters is a random process. The advantage of this method is that it can be applied to a device fabrication process and is easily prepared.

In general, a smaller contact angle is formed on the substrate (<90°) by a metal cluster than by a spherical particle (>90°). This geometrical factor can affect the growth characteristics of carbon nanotube, since the equilibrium solubility of carbon in the catalysts is a function of the curvature of radius. The metal clusters have a smaller curvature than spherical particles of the same size. This means that more carbon can be dissolved in the metal cluster than in spherical particles with same volume. As a result, nanotube growth can occur on the clusters in limited process conditions, and it may be more difficult to achieve a carbon nanotube using this technique.

2.4. Control of Growth Direction for Carbon Nanotubes

In nanoelectronic devices using carbon nanotubes, the synthesis of well aligned carbon nanotubes is desired. Carbon nanotubes are forced to grow in an upward ensemble (i.e., vertically) from the substrate. The nanotube bundle is held together by van der Waals interaction.[65] Fan et al.[11] synthesized patterned carbon nanotube bundles in vertical alignment using an electrochemically etched porous silicon. Another way to achieve vertical alignment is to use a template. Porous alumina membranes, whose pores are created by anodizing aluminum, contain vertical nanopores where carbon nanotubes grow.[66,67] The plasma enhanced CVD method, mentioned in earlier section, is a good way to achieve vertically aligned carbon nanotubes. It's advantage over other methods is

a low process temperature, which is essential to field emission display devices. Besides, it is possible to achieve straight and individually standing carbon nanotubes.[47]

To integrate nanotube-based FETs, we need a way to synthesize uniformly distributed and laterally aligned nanotubes on silicon substrates. Dai et al.[68,69] have suggested several ways to achieve lateral alignment of carbon nanotubes. Their early work suggested that CNTs could be produced parallel to the substrate by using suspended catalysts made by a lift-off process. They attributed parallel growth of nanotubes to reaction gas flow. Lateral electric fields can also be used for the same purpose.[70,71] Electric dipole polarization of the nanotubes makes them align in the applied electric field.

2.5. Other Types of Carbon Nanotube

2.5.1. Onion Like Carbon

Onion-like carbon (OLC) clusters were discovered earlier than the other types of carbon, such as fullerenes and nanotubes.[72] The electric arc is the easiest and most frequently used experiment to produce onion like carbons as well as carbon nanotubes.[73] Although this process allows a large-scale synthesis of these types of carbon nanostructures, the purification of the different components has not been easily performed. In addition to the arc discharge, the OLC has been synthesized by high temperature or irradiation induced transformation of carbon soot [74,75] or ultra dispersed diamond.[76] Recently, OLC clusters embedded in crystalline silicon carbide (SiC) using laser irradiation was reported.[77] Compared to CNTs and fullerenes, however, little is known about the electronic states and properties of OLC because of their lower availability.[78]

The morphology of OLCs shows a characteristic shape depending on the formation mechanism. Condensed phase transformation by means of irradiation annealing generates quasi-spherical shelled shapes. Ugarte et al.[79,80] showed that high electron irradiation on carbonaceous materials induced a transformation into a spherical shelled structure, which is very stable under intense irradiation. The OLCs generated by an electric arc usually show a clear polyhedral morphology and a large inner empty space.[72,81] Annealing treatment of nano diamonds produces OLCs with a remarkable spherical shape, and the morphology of the OLCs can be varied from spherical to polyhedral by controlling the annealing condition of the diamond nanoparticles.[82,83]

2.5.2. Bamboo Like Carbon Nanotube

A carbon tube with a peculiar shape looking like "bamboo," is generally called "bamboo like carbon nanotubes". The bamboo like carbon nanotubes (BCTs) were first found by Saito and Yoshikawa[84] while they were trying to fill carbon tubes with iron group metals. The typical structures in BCTs usually consist of many hollow compartments that are spaced at nearly equal separations. One end of the BCTs is usually capped with a needle-like metal particle, and the other end is empty. They have been produced by the arc discharge evaporation of graphite[85,86] or catalytic pyrolysis of hydrocarbons.[87,88]

The formation mechanisms of BCTs attributed to the catalytic effect of metal. Lee et al. [88] suggest a base growth mechanism of bamboo structure in catalytic growth of CNT using CVD. Figure 4-5 shows a schematic diagram of the growth mechanism. The mechanism contains of a sequence of following processes: 1) carbon produced from the decomposition of hydrocarbon molecules forms a graphene sheets on the metal cluster; 2) carbon is continuously added to the edge of the cap and nanotube walls grow; 3) the

compartment graphene layers grow by forming the joint with the walls; 4) the compartment layer grown on the catalytic is connected with the wall. The growth mechanism of the bamboo structure by the arc-discharge is also can be explained in similar way.[85,86]

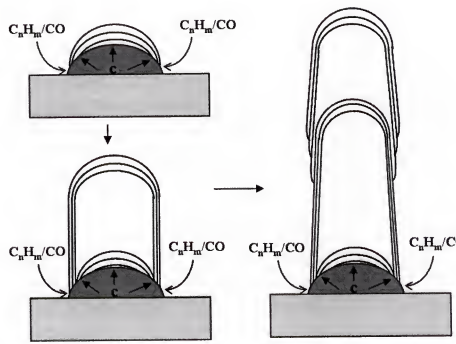

Figure 2-5. Growth mechanism of bamboo like carbon nanotubes on a substrate.

CHAPTER 3
GROWTH MECHANISM OF CARBON NANOTUBE ON NI/SIO_2 SUBSTRATE BY CATALYTIC CVD: CO CONCENTRATION MODULATION USING OXIDE POWDER IN CH_4-H_2 GAS FLOW SYSTEM

3.1. Introduction

Catalytic effect and interaction of catalyst metals with support materials have been the main concerns on growth mechanim of carbon nanotubes by CVD. The effect of oxide support has not been clearly identified yet. In this chapter, it is investigated how chemical interactions between the supporting oxide (silica) and the gas components affect the growth characteristics of CNTs. The growth mechanism of CNTs seems to be correlated to the chemical interactions between them.

Catalytic chemical vapor deposition (CVD) is a promising method for carbon nanotube synthesis because of controllability, easy scale-up and technical simplicity.[12, 47] In application of CNTs to nanoelectronic devices, direct growth of CNTs on a substrate, such as silicon wafer, makes it more difficult to produce them with a preferred property and a defined orientation. Plasma enhanced CVD[49,89,90] has been focused in synthesizing CNTs in respect of low temperature synthesis and vertical growth of them on a substrate. Several research groups[71, 91] have reported on the direct growth of CNT on silicon wafers in a controlled direction using an electric field. The chirality and the diameter of CNTs, leading to a variety of electrical properties,[5,8,9] vary with growth temperature, catalyst materials, and other growth conditions for CNT synthesis. The

control of these factors is essential in future nano electronic devices using CNTs. Unfortunately, the growth mechanism of carbon nanotubes is not well understood.

Synthesis of CNT on a silicon wafer by CVD needs to introduce catalytic metals, such as Ni, Fe, and Co. They inevitably react with under lying silicon or other underlying materials, which add another difficulty in defining the growth mechanism of CNT. The effect of supporting substrates has been received interest in the investigation of the growth mechanism of CNT. [92,93] However, the growth mechanism of CNT is still unsolved, and different results have been reported for similar process condition.

In this study, it is investigated how chemical interactions between the supporting oxide (silica) and the gas components affect the growth characteristics of CNTs. In an effort to investigate the effect of chemical components generated during the synthesis, silica (SiO_2), $SiO_2/Fe(NO_3)_3$ mixture and titania (TiO_2) were introduced to modify gas composition in the system. The effect of CO vapor concentration, which is generated from the oxides by flowing CH_4 and H_2, on the growth of CNTs will be discussed. We found that the nanotube (or nanowire) growth is greatly influenced by the kind of materials. The results could suggest a growth mechanism of CNT on oxide substrates.

3.2. Experimental

N-type silicon <100> wafers (3 Ω-cm, 2×2cm) were used as substrates for the growth of CNTs. After thermally oxidizing the substrates, nickel films (5 or 30 nm) were deposited on silicon (Si) and silicon oxide (SiO_2/Si) substrates by evaporation at room temperature. Silica (Alas Aesar, 400 mesh) and titania (Alfa Aesar, 325 mesh) were used. Silica nanoparticles (Aldrich, 8 nm) and iron nitrate mixture was prepared by mixing both in 10:1 wt% in water and drying. In this case, nano sized silica particles were adopted to

increase the interaction interface between both. Iron nitrate will form iron oxide during heating to the process temperature and will be reduced to metal in a hydrogen atmosphere.

Figure 3-1 shows a schematic diagram of the tube furnace and the relative location between the substrate and the powder in a quartz boat. The substrate (0.5×1.5 cm) is placed 2-3 cm apart from the powder in down flow. Carbon nanotubes were synthesized by CVD at 1050°C for 30 min by flowing CH_4 (10 sccm) and H_2 (200 sccm) into a quartz tube (diameter: 1.5′). The tube furnace was heated to the synthesis temperature at a heating rate of 6°C/min in Ar (800 sccm) atmosphere. The substrates were annealed for 10 min in H_2 (200sccm) at 1050°C prior to the process. After synthesis the furnace was cooled in Ar flow. The experimental conditions are summarized in table 3-1.

Table 3.1 Experimental conditions used in this study.

Powder	Substrate	Growth conditions
SiO_2	Ni(30nm)/SiO_2/Si	CH_4: 10 sccm H_2: 200 sccm Process temperature: 1050 °C
SiO_2/$Fe(NO_3)_3$		
TiO_2		
SiO_2	Ni(5nm)/SiO_2/Si	
SiO_2/$Fe(NO_3)_3$		
TiO_2		

Growth characteristics on the substrates were observed with a field emission scanning electron microscope (FESEM, JEOL 6335F) equipped with an energy dispersive spectroscope (EDS). A high resolution transmission electron microscope (HRTEM, JEOL 2010F) was used for further characterization of the CNTs. The metal

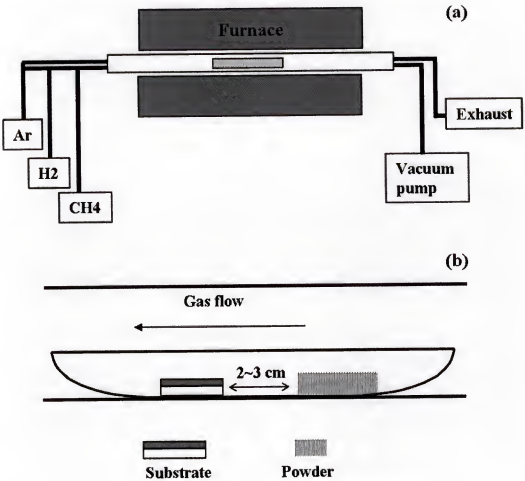

Figure 3-1. Diagram of the tube furnace (a) and the relative position between the substrate and the powder in a quartz tube (b).

and the oxide powders were annealed in same condition as the synthesis process and characterized by X-ray diffraction (XRD) and by EDS in order to investigate a chemical and a phase change of the metals during the synthesis. The thermodynamic data and phase diagram were calculated by using the "Factsage" program (Appendix A).

3.3. Carbon Nanotube Growth Characteristics

3.3.1. CNT Growth Characteristics with SiO_2 or $SiO_2/Fe(NO_3)_3$ Powder

Figure 3-2 shows a surface morphology of Ni/SiO2 substrates after the process without incorporation of a powder. It is observed that no nanotubes grow on the substrates

regardless of the metal thickness. The presence of silica particles derives a change in the growth of CNTs on Ni(30nm)/SiO_2 substrate. Figure 3-3 shows a surface

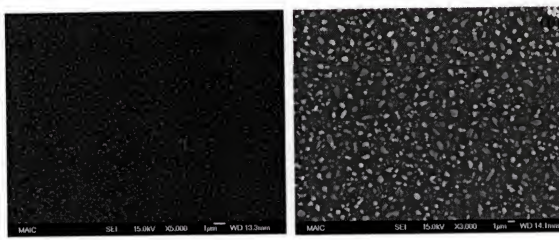

Figure 3-2. Surface morphology of the substrate after annealing in CH_4/H_2(200/10 sccm) for 30 min at 1050°C without powders: a) Ni(5nm)/SiO_2 and b) Ni(30nm)/SiO_2 substrate.

Figure 3-3. Surface morphology of the substate after annealing in CH_4/H_2(200/10 sccm) for 30 min at 1050°C on Ni(5nm)/SiO_2 a) SiO_2 powder and b) $SiO_2/Fe(NO_3)_3$ mixture.

morphology on Ni(5nm)/SiO_2 substrates using the powders. There is no change in growth behavior of CNTs with film thickness of 5 nm. On the other hand, CNTs growth is obtained on the Ni(30nm)/SiO_2 under the same growth condition. Figure 3-4 shows a surface morphology of the substrate after synthesis in presence of SiO_2 and

$SiO_2/Fe(NO_3)_3$. The Ni film broke into metal islands with diameters ranging up to 200 nm. It is observed that carbon nanotubes are grown from Ni clusters regardless of their size. It can be seen that carbon graphene layers wrap the Ni clusters.

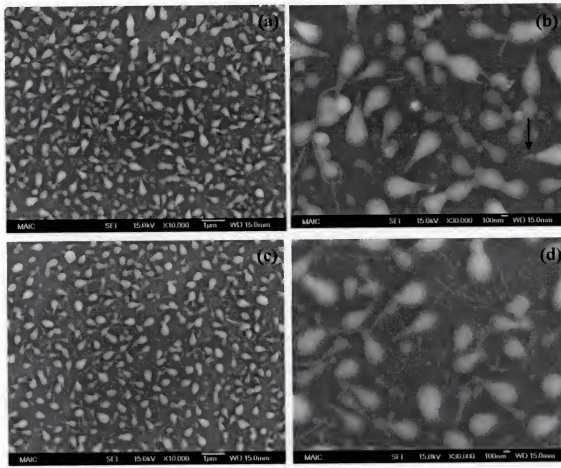

Figure 3-4. Surface morphology of the substrate after annealing in CH_4/H_2(200/10 sccm) for 30 min at 1050°C on Ni(30nm)/SiO2 substrate in presence of SiO_2 powder (a,b)and $SiO_2/Fe(NO_3)_3$ mixture (c,d).

The morphology of CNTs can be divided in two categories: one type is a conical shape generally growing from large tapered particles and the others is a straight shape having a normal CNT morphology. The average length of CNTs seems to be similar in both cases, however, the density of the straight nanotubes increases when $SiO_2/Fe(NO_3)_3$ powder is adopted. CNT grows up to about 1 μm in both cases. It is observed that a few

straight nanotubes grow from the end of the conical carbon shells, as indicated by the arrow in Fig. 3-4b. It can be observed that the density of the long and straight nanotube structure is increased when $SiO_2/Fe(NO_3)_3$ mixture.

The HRTEM analysis was carried out with a sample processed with $SiO_2/Fe(NO_3)_3$ mixture powder. A CNT in a conical shape observed on the substrates is shown in Fig. 3-5. Carbon shells completely covered the nickel cluster (diameter: 100 nm) and the tube structure extrudes out of the tapered end of the particle to form a nanotube structure. It is observed that a small nickel particle is trapped at the end of the CNT, as shown in Fig.

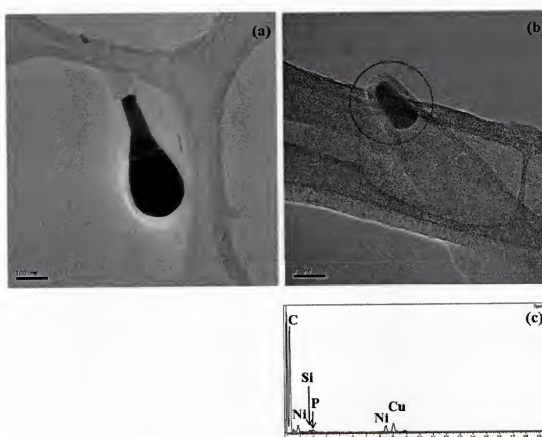

Figure 3-5. High resolution TEM photographs of a conical shaped nanotube grown on the substrate with $SiO_2/Fe(NO_3)_3$ mixture in Fig. 3-4c (a); detail structure at the tip (b); EDS spectrum from the circled area in b) (c).

5b. The EDS spectrum (Fig. 3-5c) reveals that the nanocluster is composed of Ni and small amount of Si and phosphor. The phosphor and the silicon peak in the spectrum originate from the n-type silicon substrate.

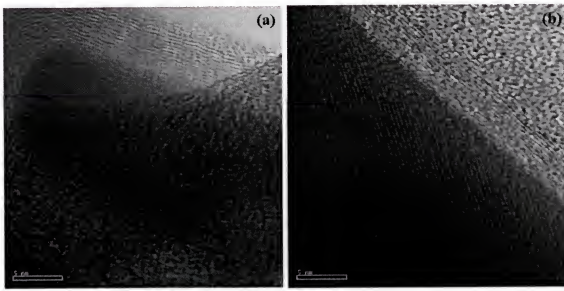

Figure 3-6. High resolution TEM photographs of the tip and the route of the nanotubes in Fig. 3-5 showing the graphene layers around the metal clusters.

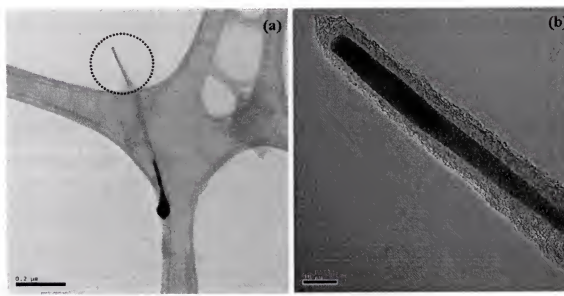

Figure 3-7 High resolution TEM photographs of the straight CNT in Fig. 3-4d. A metal nanorod is encapsulated in the nanotube cavity. The cavity size of nanotube is around 10 nm.

Figure 3-6 show a detail structure of the tip and the route of the nanotube. A straight carbon nanotube, of which length is 0.5 μm, from a small particle (40 nm) is shown in Fig. 3-7. Nickel nano clusters are observed at the tip and the route as in Fig. 3-5. However, the nickel at the tip shows nanorod morphology. It is likely that nanotube becomes thinner and longer and changes from conical to straight as the nickel cluster size decreases. EDS spectrum (not shown here) from the metal cluster showed the same chemical components with Fig. 3-5.

3.3.2. CNTs Synthesized in Presence of TiO_2

By incorporating TiO_2 powder, a change in growth behavior of CNT both on Ni(5 nm)/SiO_2 and Ni (30 nm) in presence of TiO_2 powder. The CNT growth characteristics with Ni(5 nm)/SiO_2 depend on the relative position between the substrate and TiO_2 powder. Figure 3-8 shows a surface morphology after synthesis with TiO_2. Growth density is low on Ni(5nm)/SiO_2 compared to Ni(30nm)/SiO_2. Figure 3-9a shows a bundle of nanotubes synthesized on the substrate. Even though the diameter of CNTs on Ni(5nm)/SiO_2 is similar to that of CNTs observed in Fig. 3-6, there are two differences between them: encapsulation of metal and the size of graphite cylinder cavity. The nanotubes do not contain a metal inside of them and have a smaller cavity of 1 ~ 2 nm in diameter. In addition, some onion-like carbon (OLC) structures are observed, as indicated by the arrow in Fig. 3-9b.

The nanotubes on Ni(30nm)/SiO_2 show a different morphology from those synthesized using silica particles. Figure 3-10 shows carbon structures synthesized on the substrates. The nanotubes have a bamboo type of nanotube structure and nickel clusters are contained in every cell of nanotubes. The bamboo structure has an irregular shape and

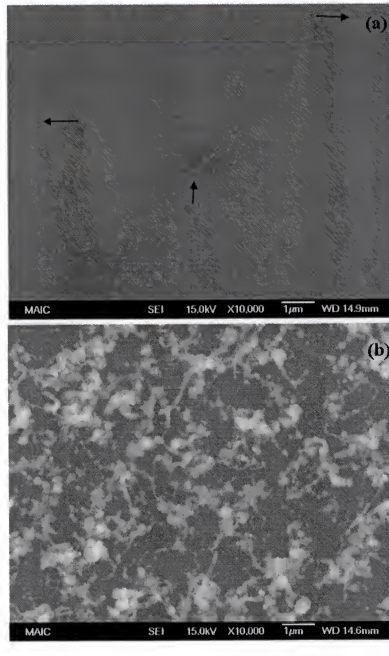

Figure 3-8. Surface morphology of the substrate after annealing in CH_4/H_2(200/10 sccm) for 30 min at 1050°C on Ni(5nm)/SiO2 substrate (a) and Ni(30nm)/SiO_2 in presence of TiO_2 powder (The arrows in (a) show example of grown nanotubes on the substrate).

the nickel inside each cell seems to act a nucleation site for new graphene layers, as shown in Fig. 3-9b. The bamboo structure seems to be derived by high CO concentration and details will be discussed in the next sections. To summarize, the morphology and

growth characteristics of CNT change with the kind of powder and the thickness of Ni film.

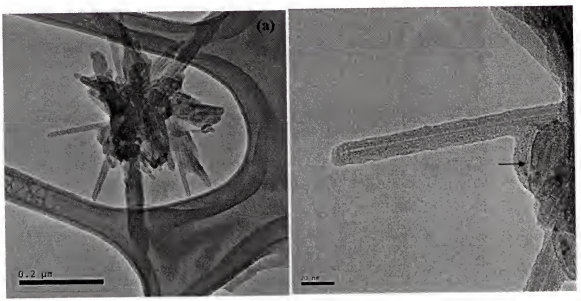

Figure 3-9. Carbon nanotube synthesized on Ni(5nm)/SiO_2 in CH_4/H_2 mixture at 1050°C in presence of TiO_2 powder. Onion-like carbon nanotubes are observed in (b).

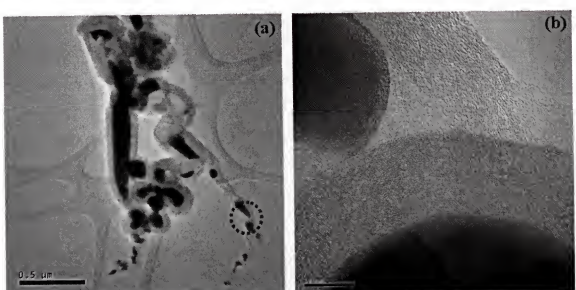

Figure 3-10. Bamboo like carbon nanotubes synthesized on Ni(30nm)/SiO2 in CH_4/H_2 mixture at 1050°C (a) and Detailed carbon structures in the circled region in a) (b).

3.3.3. Effect of the Relative Position between Substrate and TiO_2 Powder

From the results in the previous sections, carbon nano structures were observed on both substrates with TiO_2 powder. The gas decomposition rate on the oxide powders should decrease as reactions proceed. This fact can cause a change in chemical environment as the synthesis proceeds in the system. Besides, most active chemical interaction between the gas and oxide powder is expected to occur in a initial stage of process. In order to investigate the impact of chemical components generated from TiO_2 powder in a close distance, the relative position between the substrate and TiO_2 is designed as shown in Fig. 3-11.

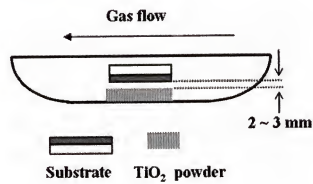

Figure 3-11. Diagram of the relative position between the substrate and TiO_2 powder, which was designed to locate both in a close distance.

The substrate was positioned 1 ~ 2 mm above TiO_2 powder. Figure 3-12 show surface morphology on a substrate (Ni:5nm). In this case, nanotube growth is only observed in the edge regions, as shown in Fig. 3-12a. Figure 3-12b and 12c show a FESEM photograph from each region in Fig. 3-12a. The structure and growth length of CNTs are different from the results in the section 3.3.2. It can be seen that nanotubes grow longer than those observed in Fig. 3-8a. In addition, bamboo like carbon nanotube structure is formed, as shown in Fig. 3-13.

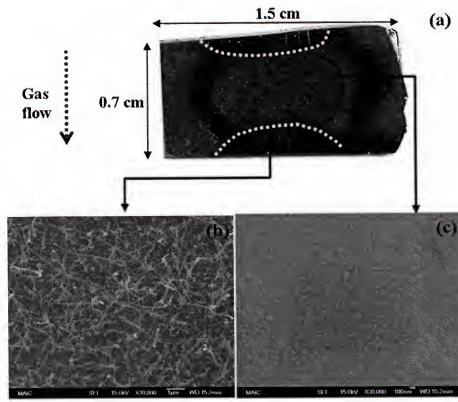

Figure 3-12. Carbon nanotube growth characteristics on Ni(5nm)/SiO_2 with TiO_2 powder: a) A photo of substrate showing a non uniform growth region of CNTs; b) a FESEM photograph from the inside of dotted line in a); c) a FESEM photograph from the center region in a).

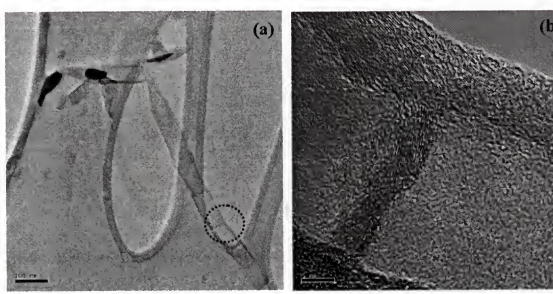

Figure 3-13. Bamboo like carbon nanotube in Fig 3-12a (a) and HRTEM photograph for the circled area in a) (b).

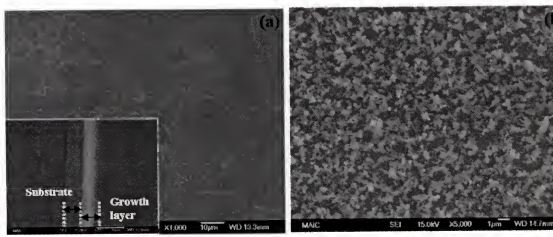

Figure 3-14. a) Field emission SEM photographs from the edge (a) and the center region (b) in case that Ni(30nm)/SiO_2 substrate is used(similar to Fig. 3-12a).

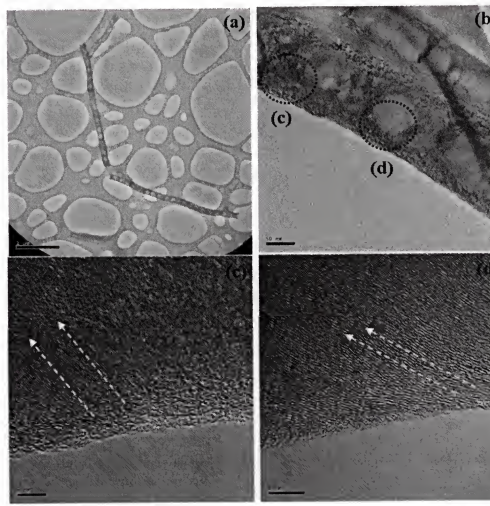

Figure 3-15. High resolution TEM photographs of a carbon nanotube in Fig. 3-14a. c) and d) are taken from the regions in b).

The growth region of carbon nanotubes on Ni(30 nm)/SiO_2 shows a similar pattern with that of Fig. 3-12a. Figure 3-14 show FESEM photographs from each region on Ni(30nm)/SiO_2. It can be observed that the nanotubes grows very long by comparing the thickness of Si substrate(675μm), as shown in the inset of Fig. 3-14a. The structure of the carbon nanotubes shows a bamboo type. The graphite layers have a different angle place to place in the nanotube, as shown in Fig. 3-15 c) and d). The growth behavior in the center region is similar to the result in the section 3.3.2.

3.3.4. Chemical and Phase Change of Oxide Powders by Annealing

In order to investigate a chemical and phase change of the powders in the CH_4/H_2 mixture, each powder was annealed in CH_4/H_2 mixture at 1050°C for 30 min. Figure 3-16 show a surface morphology of silica powder and an EDS spectrum from the powder

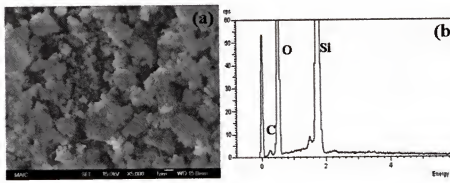

Figure 3-16. Surface morphology (a) and EDS spectrum (b) of SiO_2 powder after annealing in CH_4/H_2 (10/200 sccm) for 30 min at 1050°C.

after annealing. The EDS spectrum from the powder shows that carbon is generated on the surface of silica particles by decomposition of CH_4. CO vapor is generated by carbothermal reduction of silica particles at high temperature. CO generation increased by using $SiO_2/Fe(NO_3)_3$ mixture since CH_4 decomposition is catalyzed by Fe.

TiO_2 show a more dramatic change in composition and phase than SiO_2. Figure 3-17 show a surface morphology and an EDS spectrum after annealing in the gas mixture.

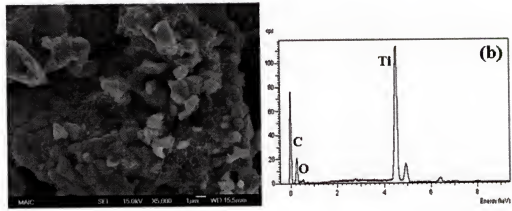

Figure 3-17. Surface morphology (a) and EDS spectrum (b) of TiO_2 powder after annealing in CH_4/H_2 (10/200 sccm) for 30 min at 1050°C.

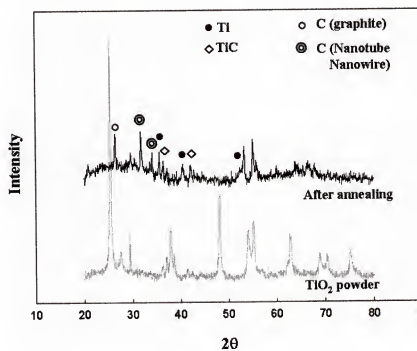

Figure 3-18. X-ray diffraction pattern of TiO_2 powder after annealing in CH_4/H_2 (10/200 sccm) for 30 min at 1050°C.

The EDS reveals that oxygen is almost removed from the powder. The XRD pattern, as shown in Fig. 18, shows that Ti and TiC (titanium carbide) and C (graphite) structure are formed during the reduction process of titania powder. It is likely that most of oxygen in the TiO_2 powder consumed by forming CO atoms. TiC can be formed by reaction of the reduced Ti with CH_4.

In addition, it can be seen that a one-dimensional nanostructure is formed on the powder, as shown in Fig. 3-17a. High resolution TEM photographs, as shown in Fig. 3-19, reveal two types of carbon structures: one is a bamboo like carbon nanotubes (BCTs) and the other is a wire composed of graphite sheets. It is observed that two types of nanowire are connected with each other, as shown in Fig. 3-19b. The details of structures are shown in Fig. 3-20. Carbon shells in the BCT have a different interplanar spacing between the side wall (2.6 Å) and the horizontal layers (3.0 Å). The wire composed of graphite sheets usually have a sheet spacing of 3.1 Å. These spacing are responsible for the peaks observed in the XRD pattern between 26° ~ 34°.

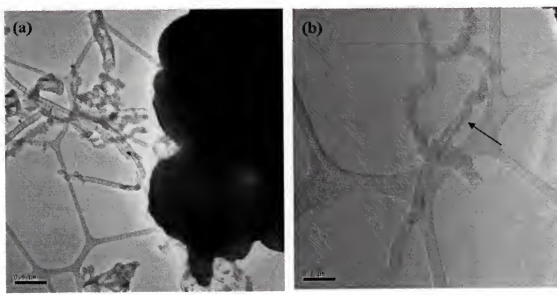

Figure 3-19. Carbon nanotube structures synthesized on TiO_2 powder during the annealing in CH_4/H_2 (10/200 sccm) for 30 min at 1050°C. The arrow in b) indicates the connected layer between the bamboo like carbon nanotube and the graphitic carbon wire.

As shown in the XRD pattern and EDS spectrum, there should exist active reactions on TiO_2 powder: the decomposition of CH_4, the generation of CO and the formation of carbon structures. The CO atoms react with CH_4 on the TiO_2 to form the carbon structures and diffuse to the substrate. The nucleation of the carbon nanostructure

can be derived by transition metal impurities in TiO_2 powder. As the reactions proceed on the surface the gas generation rate decreases due to a limited source of materials. These two different types of carbon structure seems to form in different time of process. Figure 3-21 shows a graft bamboo structure supporting observed in TiO_2 powder.

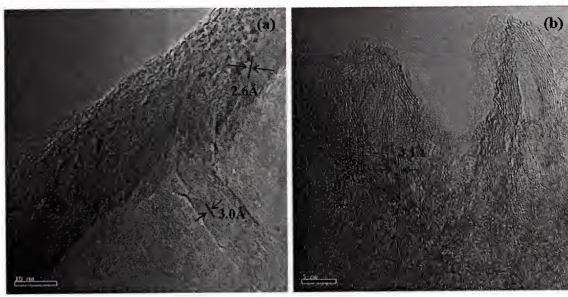

Figure 3-20. Detailed structure of a bamboo like carbon nanotube and graphitic carbon wire.

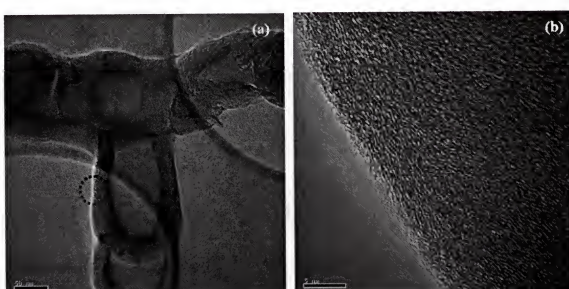

Figure 3-21. Grafted bamboo like carbon nanotubes showing that the nanotube grow by carbon condensation of vapor phase

3.4. Discussion

The growth behavior of CNTs on the substrate shows a strong dependence on the kind of oxide powder. In previous reports, the growth mechanisms of CNT by catalytic effect of the metals have been focused on the interaction between the metal and the carbon source atoms: (1) gas adsorption at the catalyst metal surface, (2) creation of a source of carbon atoms by the decomposition process by the catalyst metals, (3) dissolution in and diffusion of carbon atoms through the metal particles, (4) re-precipitation of the carbon species to form nanotube structure. [3,29-31] However, chemical interaction between gases and the support oxides have not been discussed in the growth mechanism. It could be seen that mere existence of the oxides in neighbor of the substrates can cause a dramatic change in the growth behavior of CNTs. In particular, silica is a material, which is mostly adopted as a support for CNT growth.

In the previous sections, the possibility of CO generation by reaction of the oxides or the mixture in the gas mixture was discussed. In this section, the chemical components generated from the oxides will be anticipated by thermodynamic calculation using FactSage (Appendix A). In the calculations, it is assumed that the system reaches to the equilibrium state and the gases behave ideally. The process gases, however, keep flowing thorough the tube in the experiments, which means that the calculated values do not present correct compositions. However, it is possible to anticipate gas components generated in significant amount to be considered in the system. From the calculated data (Appendix B), it is expected that CO is generated in significant amount from the powders. Other components, such as SiO and CO_2, are generated in negligible amount. CO concentration in the gas phase is increased linearly with the order of powders as

described in Fig. 17. Figure 22 shows a relative amount of CO atoms generated by interaction between the powders and the gases. (Appendix B)

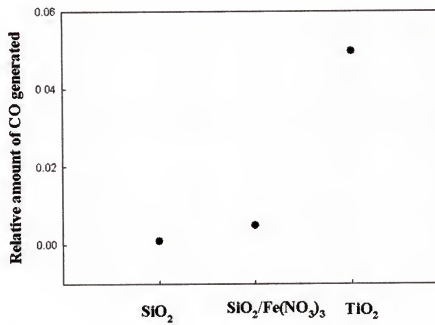

Figure 3-22. Calculated CO vapor generation from each oxide powder in CH_4/H_2(10/200 sccm) at 1050°C.

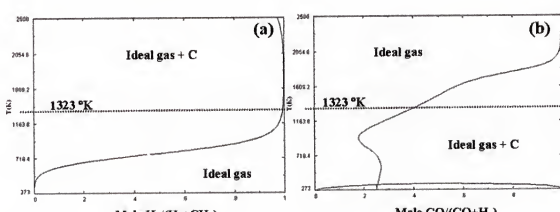

Figure 3-23. Calculated phase diagrams of CH_4-H_2 and CO-H_2 system.

The growth of CNT enhanced by CO atoms can be explained by following mechanisms. The generation of CO is a process which consumes CH_4 and generates more hydrogen molecules or atoms. Besides, CO atoms suffer self-pyrolysis at very high temperature. Rapid decomposition of carbon source gases will generate amorphous

carbon deposits on the substrates, decreasing the possibility of CNT formation. Figure 3-23 shows a phase diagram of CO-H_2 and CH_4-H_2 system.

Figure 3-24 shows calculated phase diagram for SiO_2-Ni -CH_4 and SiO_2-Ni-CO ternary system at 1050°C. The phase diagram shows an interesting effect under CO vapor system. With CH_4, it can be seen that Ni_2Si is formed in most composition range. Assuming a formation of hemispherical Ni clusters on the substrate, the nickel silicide phase is likely to from at the junction points between two solid and gas vapor phase, as shown in Fig. 3-24. Silicon is a material that can decrease the catalytic efficiency of the metal [54,55] and retard the graphitization of carbon. On the other hand, there are no silicide phases with CO gas, which means that the Ni clusters remain unaffected by silicon and active as catalysts and nucleation sites of graphene layers. The junction points, indicated as the broken circles in Fig. 25, is the locations where Ni, SiO_2 and gas vapor interact. In addition, this area is the closest points from the oxide where CO atoms are generated.

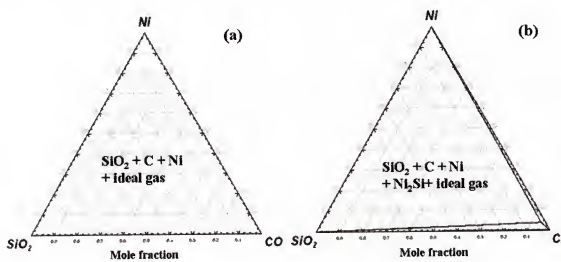

Figure 3-24. Calculated phase diagrams of Ni-SiO_2-CO (a) and Ni-SiO_2-CH_4 (b) at 1050°C.

In addition to CO vapor, it is obvious that more hydrogen exists in the middle of process since decomposition of CH_4 generates hydrogen atoms in addition to the input

gas. From thermodynamic calculations (Appendix B), it is expected that CO and hydrogen mixed atmosphere can provide a crucial impact on the growth mechanism of carbon nanotube. Figure 3-26 shows a schematic diagram showing the chemical region where carbon (graphite) can be etched in H_2-CO-C system according to H_2 amount. It is assumed that 1 mol of carbon, 1 mol of CO and H_2 (1 to 20 moles) react in 1 atm at 1323 °K. (Appendix B)

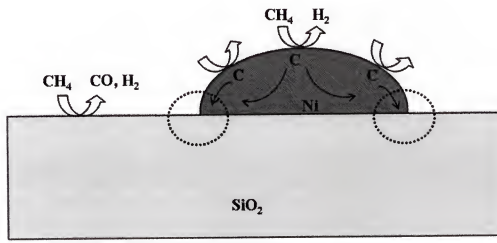

Figure 3-25. Diagram showing a chemical interaction between CH_4 and Ni or SiO_2.

It is likely that defect regions in carbon nanotubes, such as the tips, are easily etched with CO. This also implicates that it would be possible to remain the CNT tip of growing carbon nanotubes, which is very important factor in the open-ended growth mechanism of CNTs. [94] In addition, this can prevent the surface of catalyst metal capping by amorphous carbon, which make the catalysts active for a longer time.

In this experiment, the growth of CNT on thinner nickel film (5 nm) was achieved in very limited condition and the density of CNTs synthesized was very low. As the size of catalyst metals decreases the possibility which the metals are affected by reaction with supports increases. Besides, the growth temperature adopted in this study is high enough

for small Ni metal clusters to react with SiO_2 rapidly. It is known that supersaturation of carbon in metal particles and formation of cylindrical graphene layers can be easier with smaller catalyst. The growth behavior might change with lower growth temperature by using other hydrocarbon sources, such as acetylene and ethylene.

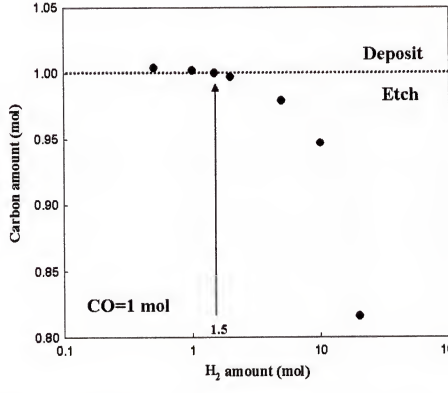

Figure 3-26. Diagram showing the etch effect of CO-H_2 components on the carbon(graphite).

3.5. Conclusions

The growth characteristics of CNTs show a strong dependence on the kind of the powders. CO vapor generated increases in order of SiO_2, $SiO_2/Fe(NO_3)_3$ and TiO_2 by thermodynamic calculation. In particular, a significant change in growth characteristics of CNT appears on $Ni(30nm)/SiO_2$ substrate. It is believed that the CO molecules play an important role in nucleation and growth of CNTs.

The growth of carbon nanotubes on Ni(5nm)/SiO_2 was not achieved easily. Low density of carbon nanotubes was grown on the substrate in presence of TiO_2 powder . The nanotubes on the substrate do not contain a metal cluster inside the nanotube. On the other hand, the growth characteristics and morphology of carbon nanotubes synthesized on Ni(30nm)/SiO_2 shows a significant change depending on the powder. Interesting carbon tube and nanowire structure were observed on TiO_2 powder after annealing in CH_4-H_2 mixture.

Silica used for the modification of gas composition is also a support in our experiment. From the result, it can be expected that there should be a chemical interaction between gas components and silica support during synthesis and the growth behavior of carbon nanotubes is influenced by the interaction. CO atoms release from oxide during the synthesis plays an important role on the growth of carbon nanotube. The relative surface area ratio between the support and the catalyst metal clusters exposed to gas phases can be a factor in growth of CNT. From these results, it becomes obvious why an oxide support, such as silica and alumina, is a crucial factor in growth of CNT by catalytic CVD.

CHAPTER 4
MODULATION OF GAS COMPOSITION BY METALLIC POWDER IN CH_4-H_2 SYSTEM AND ITS EFFECT ON THE GROWTH OF SILICON CARBIDE NANOWIRE

4.1. Introduction

In the previous chapter, it was observed that the effect of oxide powder in CH_4-H_2 gas system on the growth behavior of carbon nanotubes. In presence of the oxides in the gas, CO was actively generated from the oxide. In this chapter, metallic powder (Ti) is adopted to modify the gas composition. Ti is known to have a strong interaction with carbon. Therefore, they usually forms TiC in high temperature in CH_4 flow and release a hydrogen atoms. CO is not expected to generated in this condition, so it is to possible to investigate how the excess hydrogen can affect the synthesis of carbon nanostructures on the substrate.

Hexagon silicon carbide (α-SiC) nanowires were synthesized on the same substrate by flowing CH_4/H_2 mixture at 1050 °C in the presence of titanium, which is the same experimental condition as the chapter 3. The thickness of nickel is also a factor which affects the growth characteristics of the SiC nanowires. The density of the nanowires is dependent on the relative location of the Ti powder and the substrates. It is likely that the titanium decomposes CH_4 to form titanium carbide (TiC) and create high hydrogen concentration in the system.

Silicon carbide nanowires (SiCNWs) has been attracted much interest in nanoelectronic for high temperature, high temperature and high frequency applications.[95] Since first synthesis of SiCNWs from SiO vapor by using CNTs

templates,[96] several research groups have produced SiCNWs by using a carbothermal reduction approach,[97] a chemical vapor deposition (CVD),[98-100] and an arc discharge technique.[101] Li et al.[102] reported the direct growth of β-SiC on a silicon substrate by depositing a Cr containing SiO_x film (150nm) on it at 1300°C, suggesting a selective growth of β-SiC NWs. The growth mechanism of SiC nanowires, however, from the SiO_2 films is not clear yet. In this chapter, the growth mechanism of SiC nanowires on silica in presence of Ti powder will be discussed.

4.2. Experimental

N-type silicon <100> wafers (3 Ω-cm, 2×2cm) were used as substrates for the growth of the graphitic structure. After thermally oxidizing the substrates, nickel films (5 and 30 nm) were deposited on the silicon oxide (SiO_2/Si) substrates by evaporation at room temperature. Titanium powder (Alfa Aesar, 0.3 g, 325 mesh) and the substrate were placed in a quartz boat in two positions. Figure 4-1 shows a schematic diagram of the positions in the quartz boat. One approach is that the substrate (0.5×1.5cm) is

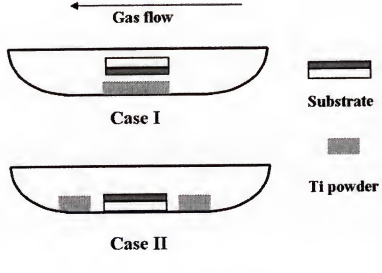

Figure 4-1. Schematic diagrams of the relative position between the substrate and Ti powder: a) case I and b) case II.

located 2 ~ 3 mm above the powder in face-down (case I). The other is that the substrate is placed between two Ti powders (case II). The quartz boat was placed in a quartz tube furnace in diameter of 1.5″. The synthesis of the nanowires was carried out in a CH_4:H_2 (10:200 sccm) gas mixture for 10 min at 1050°C. The tube furnace was heated to the synthesis temperature at a heating rate of 6°C/min in an Ar (800 sccm) atmosphere. The substrates were annealed for 10 min in H_2 (200sccm) at 1050°C prior to the synthesis.

The growth characteristics and structure of nanowires were observed with a field emission scanning electron microscope (FESEM, JEOL 6335F) and a high resolution transmission electron microscope (HRTEM, JEM 4010). Chemical analysis was carried out using an EDS equipped to the HRTEM. X-Ray diffraction (XRD) was used to investigate the phase change of titanium powder after synthesis of SiCNWs.

4.3. Growth of SiC Nanowire on Ni/SiO_2 and Growth Mechanism

Figure 4-2 shows surface morphologies of the substrates after processing: a) without Ti powder; b) in the presence of Ti powder (case II) using the substrates with Ni thickness of 30 nm. The existence of titanium powder is a crucial factor in growing SiCNWs on the silica films. No nanowires are observed on the substrate without Ti powder in our experimental condition. In this case, some carbon deposit, which is formed by the catalytic decomposition of CH_4 by Ni, is observed on the surface. The growth of nanowires is achieved on the substrate using the Ti powder, as shown in Fig. 1b. Seed metal particles are attached on the top of the grown nanowires.

TEM analysis shows the formation of α-SiC nanowires on the substrates. Figure 4-3 shows the structure and the diffraction pattern of a nanowire in Fig. 4-2b. The calculated lattice parameter from the diffraction pattern is a = 3.08 Å, which is close to

the standard data (a = 3.073Å for α-SiC). There exists an outside amorphous shell around the core SiC crystal. The chemical analysis by EDS, as shown in Fig. 4-4, reveal that the outside amorphous phase is carbon.

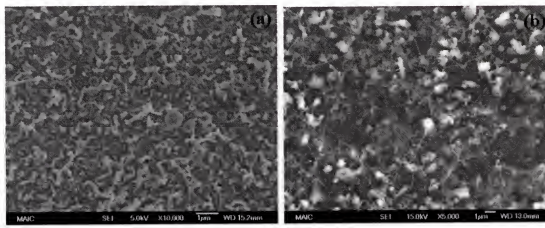

Figure 4-2. Surface morphology of the substrates after synthesis of SiCNWs for 10 min (case I): a) without Ti and b) with Ti powder. (Ni: 30 nm)

It is interesting for α-SiC to grow only in the presence of Ti powder. Carbon is supplied by carbothermal decomposition of CH_4 by Ni. Silicon is not supplied by an external source. Silicon can be supplied from the silicon oxide layers. Chemical reactions involved in the growth of α-SiC can be assumed from the chemical change of the Ti powders during the process. Figure 4-5a shows XRD patterns of the powders before and after annealing (10 min), which indicates the formation of TiC in the powder by annealing. The existence of the substrate did not affect the change in the powder. Therefore, the change in the powder phase is ascribed to the chemical interaction between the powder and the gas species in the system. TiC is formed by reaction with the decomposed carbon by Ti itself. The intensity of TiC phase in the powder is increased by increasing annealing time. As a result, the powder remains reactive and keeps functional during the synthesis of SiC nanowires.

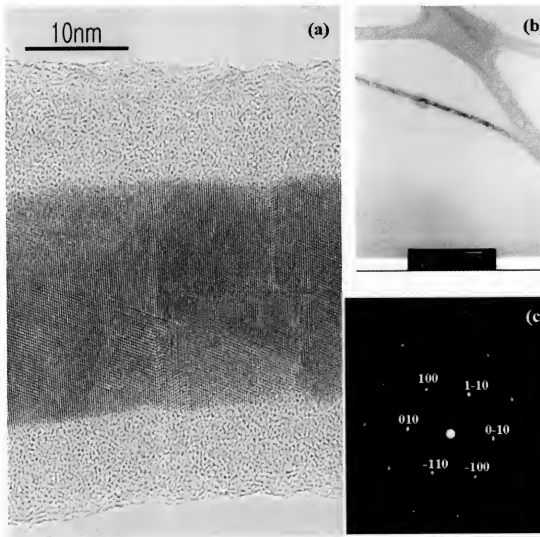

Figure 4-3. High resolution TEM of a SiC nanowire grown on the substrate in Fig. 2a (a); low magnification (b); the diffraction pattern (c).

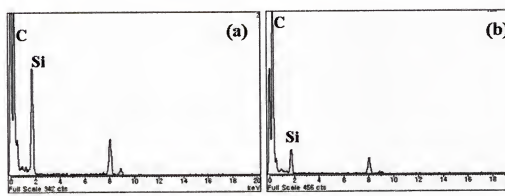

Figure 4-4. Energy dispersive spectroscopy spectra from the nanowire in Fig. 3a: a) the core and b) the outside shell.

It is obvious that the change in chemistry in the system atmosphere drives the formation of α-SiC nanowires. The growth mechanism of α-SiC nanowires can be expected from the chemical change of the powder. The surface of the silicon oxide should be a Si-rich phase by reduction in CH_4 and H_2 gas atmosphere, providing Si for the formation SiCNWs. The high hydrogen concentration created by the reaction over Ti powder expedites the reduction process at the silica surface and suppresses the self-pyrolysis of CH_4

$$CH_4 = C + 2H_2 \quad (\Delta G = -55033.8 \text{ J at } 1323°K) \qquad (4\text{-}1)$$

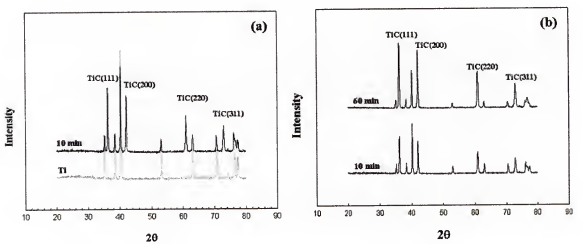

Figure 4-5. X-ray diffraction patterns for the raw Ti powder and the powder after annealing in the same condition for the SiC growth: a) comparison between the raw Ti powder and the powder after annealing in the gas mixture at 1050 °C for 10 min; b) a change in the relative intensity between the TiC and the Ti phase with annealing time.

Silicon carbide seems to form by reactions between the reduced silicon in the silica films and the decomposed carbon or CH_4

$$Si + CH_4 = SiC + 2H_2 \quad (\Delta G = -116058.9 \text{ J at } 1323 °K) \qquad (4\text{-}2)$$

Both 4-1 and 4-2 reaction is suppressed in high H_2 concentration. However, reaction (2) has a higher driving force and more favorable reaction which may occur in the growth condition. Catalytic decomposition of CH_4 on nickel clusters is also suppressed in this

respect. The experimental condition is analogous to that of synthesis of CNT. High concentration of hydrogen seems to be a key factor in the growth of SiCNWs in two respects: reduction of silica and suppression of self-pyrolysis and catalytic decomposition of CH_4. Ni islands are active sites for the nucleation of SiC (Ni particles are observed from the top end of SiCNWs observed in the FESEM photographs). Figure 4-6 shows an irregular diameter variation of the SiC nanowire in other area of nanowire in Fig. 4-3 even though that of outside shell is uniform. From this fact, it can be seen that Ni clusters do not act as a medium supplying atoms into growing nanowires as in the VLS mechanism even though they provide nucleation sites for SiC nanowires. The formation SiC nanowire seems to occur at the silica surface region by solid-solid reaction (Si-C) or solid-vapor (Si-CH_4).

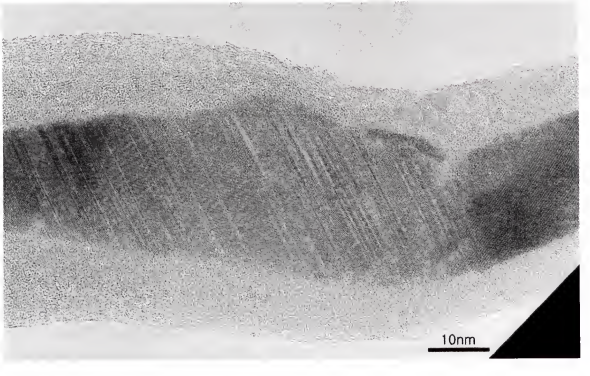

Figure 4-6. High resolution TEM photograph from another region of the nanowire in Fig. 4-3 showing the irregular size in diameter of nanowire.

Figure 4-7 shows surface morphologies of the substrates after synthesizing by the experimental set-up of case II. The growth of SiC nanowires is enhanced with Ni films of 30 nm, as shown in Fig. 6a. The dependence of growth behavior of SiC nanowires on the relative location implicates that the growth should be influenced by a local gas composition. With same experimental condition, the density of SiC nanowires is decreased using Ni films of 5nm, as shown in Fig. 4-76b. Carbon concentration, which is generated by Ni, decreases with decreasing the film thickness. As a result, the capability both in reducing silica layer and supplying carbon for the formation of SiC seems to be reduced in such a case.

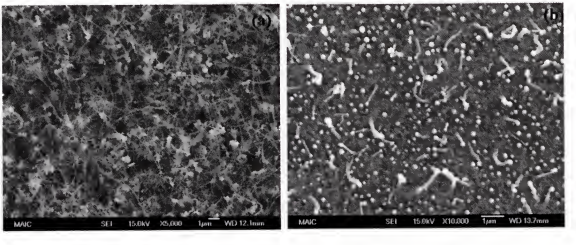

Figure 4-7. Silicon carbide nanowire growth characteristics on the substrate using case II position: a) 30 nm Ni and b) 5nm Ni.

4.4. Conclusion

Hexagonal silicon carbide (α-SiC) nanowires were synthesized on silica films by flowing methane and hydrogen mixture at 1050°C in the presence of titanium. In the presence of Ti powder, no carbon nanotubes were synthesized on the substrates. The growth characteristics of SiC depend on the relative location between the substrate and Ti powder and Ni film thickness. TiC is formed in the Ti powder by reaction with carbon

from decomposed CH_4 by Ti itself, which leads to a high hydrogen concentration in the system. It seems to create a highly favorable environment for the formation of SiC by reducing silica films and suppressing the self-pyrolysis of and catalytic decomposition of CH_4.

CHAPTER 5
CARBON NANOTUBE TIP STRUCTURE CHANGE AND ONION LIKE CARBON STRUCTURES NUCLEATED ON CARBON NANOTUBES BY THERMAL TREATMENT WITH OXIDE POWDER IN CH_4-H_2

5.1. Introduction

In chapter 3, the effect of oxide materials on the growth characteristics of carbon nanotubes on Ni/SiO_2 substrate was investigated. And, several mechanisms for the enhanced growth of CNTs in the presence of oxide powder were discussed. In this chapter, CNTs are annealed in the presence of the oxide powder in CH_4-H_2 gas flow at the synthesis temperature in order to investigate the effect of the oxides on growing carbon nanotubes. The oxide powders and the CNTs were not in contact each other. By investigating the structural changes in CNTs, the effect of oxide materials on the growth mechanism of CNTs will be discussed. In addition, onion like carbon structure was observed on the CNT walls during the annealing process. Onion-like carbon (OLC) clusters were discovered earlier than the other kinds of carbon, such as fullerenes and nanotubes.[103] Onion-like carbons have been synthesized by high temperature or irradiation induced transformation of carbon soot [74,75] or ultra dispersed diamond.[76] Recently, OLC clusters embedded in crystalline silicon carbide (SiC) by using laser irradiation was reported.[77] The formation mechanism of OLC will be discussed with regard to the tip structure change CNTs.

5.2. Experiment

Silica (SiO_2, Alas Aesar, 400 mesh,) and titania (TiO_2, Alfa Aesar, 325 mesh) and silica/iron nitrate($Fe(NO_3)_3$, Aldrich, anhydrous) were adopted. Silica nanoparticles

(Aldrich, 8 nm) and iron nitrate mixture was prepared by mixing both materials in 10:1 wt% in water and drying. In this case, nano sized silica particle was adopted to increase the interaction interface between two materials. Iron nitrate will reduce to iron oxide during heating to the process temperate and reduced to metal in a hydrogen atmosphere.

The oxide powder (0.3 g) and multi-wall CNTs (0.01 g) were placed in a quartz boat. The powder was located in the up-flow at a distance of 2 to 3 cm from the CNT powder. Figure 5-1 shows a schematic diagram of the relative positions between them. Ar gas (800 sccm) kept flowing during the heating and cooling after annealing to prevent oxidation of CNTs. The tube furnace was heated to the annealing temperature at a heating rate of 6°C/min. The system was pre-treated in Ar:H_2 (150:200 sccm) for 10 min at 1050°C prior to flowing CH_4. Annealing of CNTs was carried out for 1 hr in CH_4:H_2 (10:200 sccm) at 1050°C.

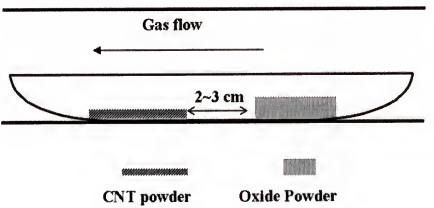

Figure 5-1. Schematic diagram of relative position between the substrate and the powder in a quartz tube.

The structures of the pre- or post- annealed carbon nanotubes were observed using a high resolution transmission electron microscope (HRTEM, JEOL 2010F) equipped with an energy dispersive spectroscope (EDS). Thermodynamic data were calculated using the "Factsage" program.

5.3. Results and Discussion

Figure 5-2 show typical tip structures of MWCNT observed prior to the annealing. The original structures of the tip have round (1a) or conical shape (1b and 1c). Figure 5-2c shows a bamboo like tip structure formed at the tip of CNT. The tips of CNTs are restructured after annealing process. Figure 5-3 show two tip morphologies of CNT observed after annealing in presence of silica, $SiO_2/Fe(NO_3)_3$ or TiO_2 powder, showing the polyhedral structures. A open tip structure of CNT was observed with annealing TiO_2, as shown in Fig. 5-3d.

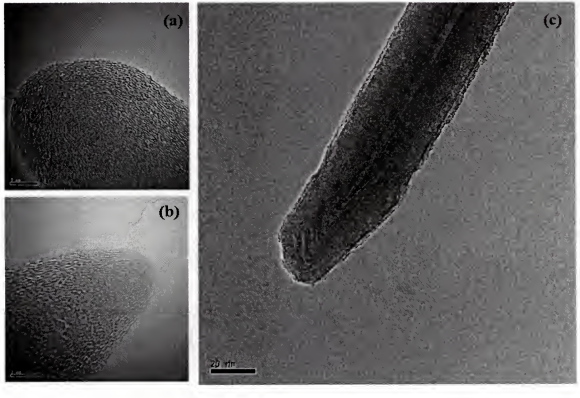

Figure 5-2. Tip morphologies of CNTs before the annealing treatment.

In addition to the change in the tip structure, OLCs are nucleated on CNTs simultaneously. However, the OLC structures were observed in low density with SiO_2 and TiO_2. Therefore, the results will be described in detail for $SiO_2/Fe(NO_3)_3$ mixture powder. Figure 5-4a shows a TEM photograph of a CNT after annealing CNTs in

presence of the mixture. The dark regions or the humps represent OLCs nucleated on the CNTs. HRTEM photographs from several spots, as shown in Fig. 5-4b, 5-4c, and 5-4d, reveal the various carbon structures nucleated on the CNT. The OLCs generally have spherical shapes, which is similar to the morphology of OLCs by the irradiation method. The size of the OLCs is not uniform, as shown in Fig. 5-4a and 5-4b (indicated by the arrows).

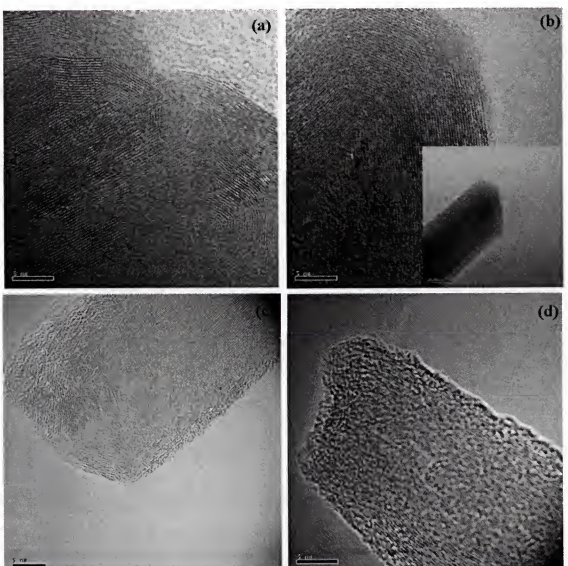

Figure 5-3. Tip morphologies of CNTs after annealing in presence of SiO_2 (a), $SiO_2/Fe(NO_3)_3$ (b) or TiO_2(c,d) at 1050°C.

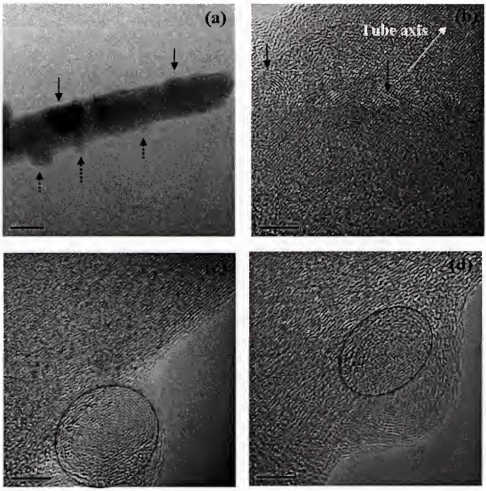

Figure 5-4. High resolution TEM photographs showing OLCs nucleated on CNTs after annealing in CH_4:H_2 (10:200 sccm) gas mixture at 1050°C. a) A low magnification photograph of the CNT. The darker regions indicate OLC graphitic structures located on the top of CNTs, making a overlapping image; b) A HRTEM photograph representing OLCs from a darker part in a). Since the graphitic image is overlapping with CNTs and a amorphous carbon layer, the image is not clear in case of the larger one; c) and d) HRTEM photographs of OLCs not overlapping with the CNT, indicated as the broken arrows in a).

Different morphologies of OLCs were observed in this experiment, such as polyhedral tubular shapes, as shown in Fig. 5-5. The tubular graphitic carbon grows along the tube axis of the CNT. It can be seen that an amorphous layer covers the tubular structure. Figure 5-6a and 5-6b show an OLC nucleated between two carbon nanotubes, forming a network structure of them. The shape of the OLC reveals that the graphite layers of the OLC growth along the side walls of two CNTs. Amorphous carbon layers

are normally observed on the side wall of CNTs except that SiO_2 powder is adopted, as shown in Fig. 5-7. The EDS spectrum (Fig 5-7d) from the Fig 5-7b confirms that the amorphous is composed of carbon only.

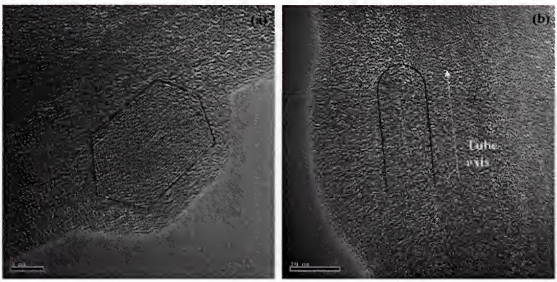

Figure 5-5. High resolution TEM photographs showing different structures of OLC observed in this experiment using $SiO_2/Fe(NO_3)_3$ powder: a) polyhedral and b) tubular structure.

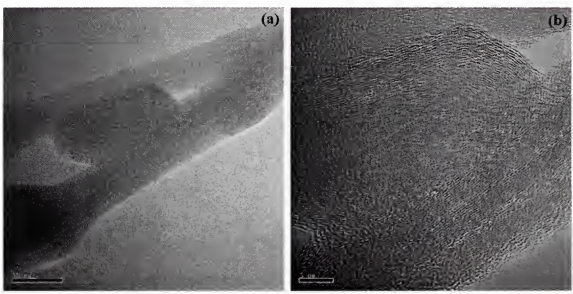

Figure 5-6. Onion like carbon structure nucleated between two CNTs: a) a low magnification TEM; b) a HRTEM photograph.

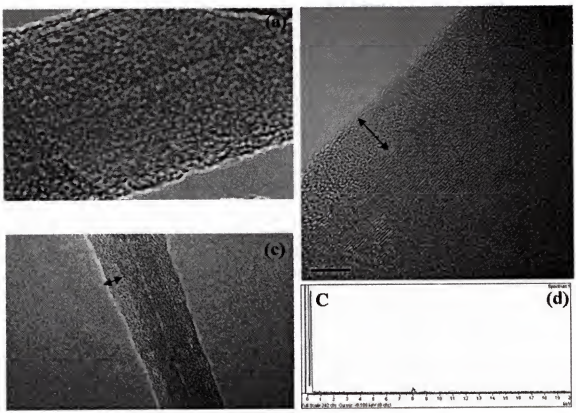

Figure 5-7. Amorphous layer deposited on the side wall of CNTs after annealing in presence of a) SiO_2, b) $SiO_2/Fe(NO_3)_3$ and c) TiO_2 powder. It can be seen that there is no amorphous layer on the side wall treated with SiO_2. d) The EDS spectrum from the Fig. 7b.

The formation of the carbon structures on the side wall of CNTs and the change of tip morphologies can be ascribed to a chemical change in the system, which is derived by the existence of the powders. Thermodynamic calculations using the program reveal that carbon monoxide (CO) is the most component generated from the oxide powders in CH_4-H_2 flow mixture at the annealing temperature. It is obvious that more hydrogen exists in the middle of process since decomposition of CH_4 generates hydrogen atoms in addition to the input gas. A question is that how much percentage of atomic hydrogen exists in the system. This seems to be an important factor in understanding the phenomena observed in this experiment.

Figure 3-17 shows the equilibrium CO concentration calculated in each case. It can be seen that CO concentration increase in order of SiO_2, $SiO_2/Fe(NO_3)_3$ and TiO_2 powder. The calculation assumed that 1 mol of each powder, 1 mol of H_2 and 0.05 mol of CH_4 react at 1050°C. The CO generation can be occurred by following reactions:

$$SiO_2(s) + C(s) \rightarrow SiO_{2-x}(s) + CO\ (v) \quad (5\text{-}1)$$

$$TiO_2(s) + C(s) \rightarrow TiC(s) + Ti(s) + CO\ (v) \quad (5\text{-}2)$$

XRD diffraction analysis revealed that C, Ti and TiC phases exist after annealing TiO_2 in the mixture gas at 1050°C (Fig. 3-13). $SiO_2/Fe(NO_3)_3$ generates CO molecules 5 times as much as silica powder in CH_4-H_2(10/200 sccm), and TiO_2 generates CO molecules 10 times as much as $SiO_2/Fe(NO_3)_3$. The concentration of atomic hydrogen can be expected to increase in same way with CO concentration since CO is formed by decomposition of CH_4.

The etch effect of CO-H_2 gas component on carbon(graphite) has already been discussed in the chapter 3. It is interesting that CO plays a very important role in etching of carbon but high concentration of CO leads to a deposit of carbon. The tip of CNTs is a region where there exist a disordered carbon structure and a higher curvature than the side wall. As a result, the carbon atoms can be removed from the tip preferentially in relatively low CO and high H_2 concentration. In similar way, defective points at the side wall of CNT can be etched preferentially, giving active sites for the nucleation of OLC structures.

In presence of TiO_2, CO generation rate seems to be too rapid, which results in the amorphous carbon deposits by decomposition of carbon source gases before OLCs nucleate on the side wall of CNTs. The restructuring at the tip implicates that the end tip

of CNTs is easily attacked by the chemical species generated during the annealing. This also implicates that it would be possible to remain the CNT tip of growing carbon nanotubes, which is very important factor in the open-ended growth mechanism of CNTs.[94] Silica used for the modification of gas composition is also a support normally adopted for the growth of CNT by catalytic CVD. From the result, it can be expected that there should be a chemical interaction between gas components and silica support during synthesis. It is likely that the CNT growth behavior is influenced by the interaction.

5.4. Conclusion

In summary, the tip structures of CNT were modified by annealing in presence of SiO_2, $SiO_2/Fe(NO_3)_3$ and TiO_2 powder in CH_4-H_2 flow. Onion like graphitic structures were nucleated on the side of the CNTs at the same time. The morphology of OLC can be modified from spherical to polyhedral by changing gas composition. The powders in CH_4-H_2 seem to generate chemical species, such as CO and atomic hydrogen, which are effective etchants for carbon. They attack defective sites in CNTs, such as the tips, preferentially and cause the change in tip morphologies. The nucleation of OLCs on the side wall of CNTs can be explained by similar mechanism. The results can be correlated with those in chapter 3.

CHAPTER 6
CONTROL OF GROWTH ORIENTATION FOR CARBON NANOTUBES

6.1. Introduction

Carbon nanotubes (CNTs) growth on silicon substrates in controllable ways is a challenge for use in nano-electronic devices. Vertically aligned CNTs have been produced by using chemical vapor deposition (CVD) over catalyst particles patterned on a porous substrate[11], and on a glass substrate by plasma enhanced CVD.[49] There is a general tendency for CNTs to form bundles as they grow, which makes it difficult to interpret their growth mechanism.

In this chapter, it will be suggested how to control of growth orientation for CNTs the silica substrate by CVD. Assembly of laterally aligned CNTs on silicon oxide substrates was achieved on iron catalyst particles on silica substrates. The iron nano particles were adhered onto the substrates from dispersion by applying magnetic fields to the iron nanoparticles. Magnetic anisotropy tends to force the magnetization into a well defined direction, called easy axis. As a result, it is expected that single crystal iron nano particles can be arranged on the substrate with one crystallographic orientation by magnetic field. In this chapter, aligned carbon nanotubes were also synthesized vertically or with tilt angle to the substrates by changing the angle between the substrate and the magnetic field direction. The best alignment of carbon nanotubes is usually produced closer to the edge of the substrates.

The growth direction of CNTs could be correlated with the applied magnetic field, i.e. the growth direction is approximately perpendicular to the magnetic field. This result

suggests the possibility to control the growth orientation of the CNTs. Furthermore, novel evidence is given for the growth mechanism of the CNTs from the metal catalyst particles by CVD.

6.2. Experimental

6.2.1. Preparation of Iron Nanoparticles

Iron catalyst nanoparticles were prepared by thermal decomposition of an organometallic precursor ($Fe(CO)_5$) in melted trioctylphosphine oxide (TOPO).[104] The nanoparticle synthesis process was slightly changed from the previously reported method. A 0.2 mL of $Fe(CO)_5$ was added to 6.0g of trioctylphosphine oxide(TOPO) at 330°C under argon atmosphere, and then aged for 30 min at the same temperature. The reaction mixture was added to excess ethanol and centrifuged several times. Transmission electron microscopy analysis showed that single crystal iron nanoparticles with diameter of 5 nm were synthesized. Iron nanoparticles were dispersed in hexane, and adhered on the substrate before growing carbon nanotubes.

6.2.2. Attachment of Iron Nanoparticles on the Substrate

A magnetic bar (140 mT) was used for adhering iron particles on the substrate from solution. N-type (resistivity: 3 Ωcm, thickness: 625 μm) silicon (100) wafers with thermal oxide film (250 nm) were used as substrates. Substrates were attached to the magnetic bar in two different positions, case 1 and case 2 as shown in Fig. 6-1, followed by dipping into the dispersed iron nanoparticles slurry for 1 to 2 seconds directly after sonicating the dispersion. Iron nanoparticles have a strong tendency to agglomerate because of their magnetic characteristics and high specific surface energy. Therefore, the slurry is ultra-sonicated before dipping the substrates. The magnetic bar was removed from the substrate after complete evaporation of the solvent.

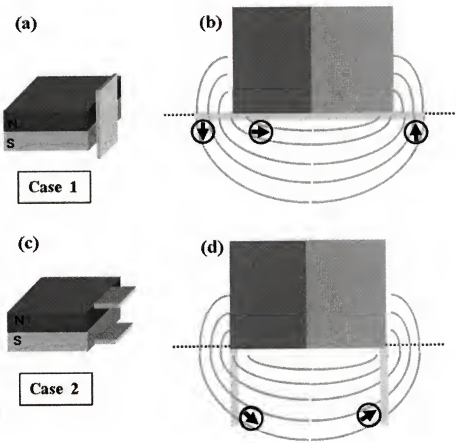

Figure 6-1.Schematic diagram of a magnetic bar used for adhering iron nanoparticles to the silicon substrates. (Circled arrow shows the orientation of the easy axis of the iron nanoparticles) (a) The substrate is attached parallel to the side of the magnetic bar in case 1. (b) The simplified magnetic field around the substrate in case 1. The field is perpendicular at the edge, and parallel at the center. (c) The substrate is attached perpendicular to the side of the magnetic bar in case 2. (d) The simplified magnetic field around the substrate in case 2. The magnetic field tilts to the substrate.

6.2.3. Carbon Nanotube Growth

Then carbon nanotubes were grown at 1050°C using argon, methane, and hydrogen gas with flowing speeds of 1000, 50, and 50 sccm, respectively. A quartz tube that is 1.5 inches in diameter and 48 inches in length was used for the CVD furnace. The substrate temperature was increased by 6°C/min up to the growth temperature in argon atmosphere with a flowing speed of 600 sccm. On reaching growth temperature, the furnace temperature was held constant for 10 min, then annealed in hydrogen (50sccm) and argon

(1000sccm) before growing the CNTs. After growing the CNTs, the furnace was cooled to room temperature in argon (600sccm). The growth orientation of carbon nanotubes were observed using a field emission scanning electron microscope (FESEM).

6.3. Growth Behavior of Carbon Nanotubes on Magnetically Aligned Fe Nanoparticles on the Substrates

Scanning electron microscopy (SEM) was used to examine carbon nanotubes grown on silicon oxide substrates. Figure 6-2 shows low magnification scanning electron microscope (SEM) images of nanotubes grown from case 1 in Fig. 6-1. Figure 6-3 shows the 4 distinct locations of CNT growth as observed by SEM. In region (a) and (b) carbon nanotubes appear to grow laterally and in alignment with the substrate (Fig. 6-2 (a), (b)). On the side wall of substrate (Fig. 6-2 (c)), where the magnetic field is parallel to the surface, the CNTS grew vertically on the surface. Figure 6-2 (d) also shows vertically grown CNTs in the center region with parallel magnetic field lines to the substrate surface.

In the work presented here, the reaction gas flow was perpendicular to the silicon wafer, i.e. perpendicular to the growth direction of CNTs in regions (a), (b), (c), and (d), which means that the growth direction of the CNTs is not derived by gas flow. Compared to vertical growth, which allows unlimited space for growing, laterally growing carbon nanotubes will overlap with each other if their length exceeds the space between the iron nanoparticles. As a result they may form bundles or some CNTs' growth direction will be deflected away from the original growth orientation, as observed in Fig. 6-2 (b).

For case 2 (see Fig. 6-1) the substrate were attached vertically onto the magnetic bar for dip coating. Here, growth of aligned CNTs tilting from the substrates is found as shown in Fig. 6-4 (a), (b), and (c). They appear to arch over the substrate which is

assumed to be caused by the weight of the catalyst particle at the "top" of the growing CNT. Figure 6-4 (d) shows a schematic diagram for the suggested growth mode. As in case 1, the tilted CNTs grow in the same orientation-relation to the magnetic field, and the region with the best CNT alignments are found closest to the edge of the substrates.

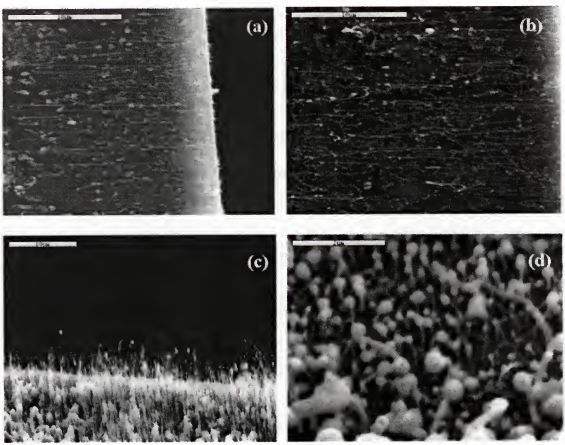

Figure 6-2. Morphology of carbon nanotubes grown on the substrate in Case 1. The carbon nanotubes were synthesized at 1050°C for 10min. (a) The CNTs grow laterally with alignment at the edge. (b) CNTs overlap with each other during the growth when a large number of CNTs are grown in a small area. (c) Carbon nanotubes grow vertically at the side wall region of the substrate. (d) Vertical growth of CNTs at the inside region of the substrate (d) region of Fig. 2 (e), showing top growth mode (SEM tilt angle is 45°).

Several exciting phenomena were observed in relation to the growth orientation of CNTs and the applied magnetic field. First CNTs have a tendency to grow approximately perpendicular to the applied magnetic field lines as is shown in Figure 6-2 for regions (a),

(b), (c), and (d). Second the alignment of CNTs is usually observed close to the edge of the silicon wafer. Third the growth direction of CNTs is dependent on the boundary shape of the edge.

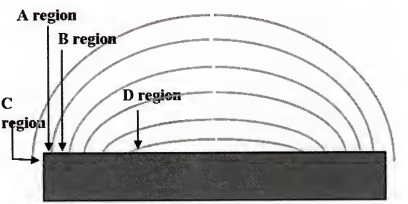

Figure 6-3. Schematic diagram showing the position observed in (a), (b), (c), and (d) respectively. The opposite side of the substrate shows the same trend in the growth characteristics.

In our work, the CNTs were produced at 1050°C, which is much above the Curie temperature of iron (770°C). The iron nanoparticles are demagnetized at the growth temperature; as a result, the magnetic effect of the iron particles on the growth characteristics could be excluded. We suppose that the most probable reason for these phenomena should be related to the crystallographic orientation of iron nanoparticles. Magnetic anisotropy tends to force the magnetization into a well defined direction. Uniaxial anisotropy favors alignment of the magnetization along an easy axis. Ferromagnetic materials, such as iron, nickel and cobalt, have one crystallographic easy axis. For example, iron (bcc) favors magnetization parallel to the <100> direction. The easy axis tends to be parallel to the magnetic field. As a result, the applied magnetic force fixes the adhering particles to a defined orientation on the substrate (Fig. 6-1 (c), (d)).

Regardless of the phase transition of the iron nanoparticles, they seem to maintain a discrete crystallographic orientation at the CNT growth temperature. From the results, it

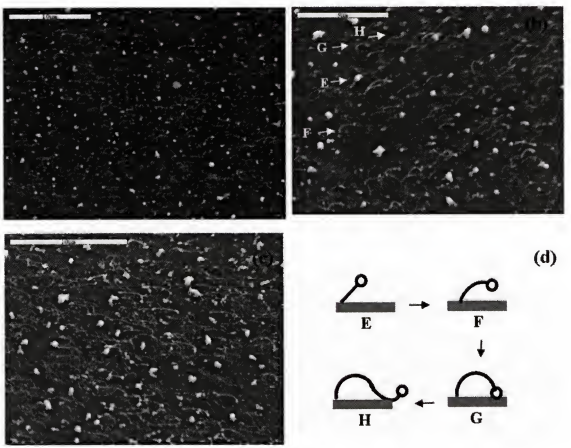

Figure 6-4. Morphology of CNTs grown on the substrates in Case 2 (SEM tilt angle is 45°). The carbon nanotubes were synthesized at 1050°C for 10min. All of them have an arch-like shape and grow in the same direction. (a) (b) SEM shows that CNTs grow in the same direction over a large area (N pole side in Figure 1 c). (C) SEM photograph of CNTs grown at S pole side in Fig. 1 c. (d) Schematic diagram of the shapes of CNTs produced in (a), (b), and (c). The CNTs have several shapes according to the growth length (each case is indicated in (b)).

is assumed that the CNTs grow along a certain crystallographic orientation or plane that is about perpendicular to the easy axis. However, at least two orientations should be fixed in order to arrange 3-dimensional nanoparticles on a defined direction. One orientation, that is the easy axis, should be fixed parallel to the magnetic field direction. An inhomogeneous magnetic field possibly could fix the other orientation. Magnetic field

lines are deflected at the boundary of the silicon substrate, which is diamagnetic, resulting in an inhomogeneous field in this region. Iron nanoparticles arranged themselves so as to minimize the magnetic anisotropy energy in an inhomogeneous field. This could explain why alignment of carbon nanotubes is achieved in the edge region and the growth direction of the CNTs were affected by boundary shape in this region. In this work, it was observed that the orientation of the CNTs' growth is strongly dependent on the inhomogeneous character of the local magnetic field providing an inhomogeneous magnetic field.

As a matter of fact, there exists a strong magnetostatic interaction between magnetized nano particles due to their external magnetic field. In our work, the magnetic bar was removed from the substrates after drying the sample. While dipping the substrates into the dispersion, most of the particles were concentrated in the region of high magnetic field. In this region, the magnetostatic interaction between the iron nanoparticles may have forced them deflect each other after the magnetic bar was removed from the substrate.

Nanoparticles which are in contact with each other aggregate during heating to form larger particles, which delay or prevent the growth of CNTs. In addition to this, the tendency of the CNTs to form bundles makes it more difficult to maintain the original growth orientation. As a result, the relationship between the growth direction of the CNTs and the applied magnetic field is less obvious in this region.

The results thus indicate a correlation between the growth direction of the CNTs and the crystal orientation of the catalyst particles. Until now, there has been much controversy about the growth mechanism of CNTs. These findings may suggest a

solution to a fundamental question in growth of CNTs and the parameters that determine CNT growth direction over, and orientation relative to, catalyst materials. The finding that the orientation of CNTs can be varied with a magnetic field indicates the following i) nanotubes must grow from defined crystallographic facets of the iron nanocrystals, ii) the catalyst particle stays aligned with the magnetic field beyond its Curie temperature of 770°C, and iii) the iron nanoparticles are not a liquid catalyst but a solid material that dissolves and reprecipitates carbon.

This study focused on iron particles, but similar principles may apply to other catalysts such as cobalt and nickel that have different crystal structures and easy axis for magnetization. Finally, this work shows that it is possible to produce laterally aligned CNTs on silicon wafers naturally, which increases the ability of CNT integration in nano-electronic devices.

6.4. Conclusion

Laterally aligned carbon nanotubes were synthesized on substrates over iron nanoparticles by using chemical vapor deposition. In addition, aligned carbon nanotubes grown vertically and with tilt angle to the substrates were produced, which means that it is possible to grow aligned carbon nanotubes at any angle relative to the substrate. The growth direction of the carbon nanotubes was controlled by a magnetic field that is applied in the process of adhering catalyst particles on silicon oxide substrates from dispersion.

The ferromagnetic property of the iron nanoparticles fixes them in a defined orientation under magnetic field, which results in aligned growth of the carbon nanotubes. These results indicate that carbon nanotubes preferentially grow from certain facets of the catalyst particles, suggesting a crucial clue in investigating the growth mechanism of

carbon nanotubes. The laterally aligned carbon nanotubes could make it possible to integrate them in nano-electronic devices, such as a channel for field effect transistors.

CHAPTER 7
CONCLUSIONS

The growth characteristics of CNTs show a strong dependence on the kind of the powders. CO vapor generated increases in order of SiO_2, $SiO_2/Fe(NO_3)_3$ and TiO_2 by thermodynamic calculation. In particular, a significant change in growth characteristics of CNT appears on $Ni(30nm)/SiO_2$ substrate. It is assumed that CO plays an important role in nucleation and growth of CNTs. The growth of carbon nanotubes on $Ni(5nm)/SiO_2$ was not achieved easily. Low density of carbon nanotubes was grown on the substrate in presence of TiO_2 powder . The nanotubes on the substrate do not contain a metal cluster inside the nanotube. On the other hand, the growth characteristics and morphology of carbon nanotubes synthesized on $Ni(30nm)/SiO_2$ shows a significant change depending on the powder.

Silica used for the modification of gas composition is also a support in our experiment. From the result, it can be expected that there should be a chemical interaction between gas components and silica support during synthesis and the growth behavior of carbon nanotubes is influenced by the interaction. CO atoms release from oxide during the synthesis plays an important role on the growth of carbon nanotube. The relative surface area ratio between the support and the catalyst metal clusters exposed to gas phases can be a factor in growth of CNT. From these results, it becomes obvious why an oxide support, such as silica, alumina and zeolite, is a crucial factor in growth of CNT by catalytic CVD.

Hydrogen concentration is assumed to affect the growth of carbon nanotubes and silicon carbide nanowires. It is difficult to estimate hydrogen concentration since they will form by the reactions on the oxide and decomposition of methane on the catalyst metal. By incorporating metallic powder instead of oxide powder, a different nanostructure grows on the type of substrate.

Hexagon silicon carbide (α-SiC) nanowires were synthesized on silica films by flowing methane and hydrogen mixture at 1050°C in the presence of titanium. The growth characteristics of SiC depend on the relative location between the substrate and Ti powder and Ni film thickness. TiC is formed in the Ti powder by reaction with carbon from decomposed CH_4 by Ti itself, which leads to a high hydrogen concentration in the system. It seems to create a highly favorable environment for the formation of SiC by reducing silica films and suppressing the self-pyrolysis of and catalytic decomposition of CH_4.

Tip structures of CNTs were modified and OLCs were formed on CNTs by annealing the CNTs with the oxide powders. The morphology of OLCs showed spherical and polyhedral shapes Interconnection structures were formed by onion like carbons between two CNTs. The OLC junction could lead to a way forming an electrical junction and a network structure of CNTs. The surface structure observed in this experiment shows that the onion graphite layers are nucleated from vapor. In addition to CO vapor, it is assumed that more hydrogen exists in the middle of process since decomposition of CH_4 generates hydrogen atoms in addition to the input gas. It seems that new graphene walls nucleate on defect points of on carbon nanotubes in high CO concentration.

The restructuring at the tip implicates that the end tip of CNTs is easily attacked by the chemical species generated during the annealing. This also implicates that it would be possible to remain the CNT tip of growing carbon nanotubes, which is very important factor in the open-ended growth mechanism of CNTs. Silica used for the modification of gas composition is also a support normally adopted for the growth of CNT by catalytic CVD. From the result, it can be expected that there should be a chemical interaction between gas components and silica support during synthesis. It is likely that the CNT growth behavior is influenced by the interaction.

In summary, the growth of CNT enhanced by CO atoms can be explained by the following mechanism. The generation of CO is a process which consumes CH_4 and generates more hydrogen molecules or atoms. This will retard the decomposition rate of CH_4 on the metal catalyst. Besides, CO atoms suffer self-pyrolysis at very high temperature. In brief, the function of the oxide powders is to delay the decomposition of hydrocarbon source gas. This prevents a rapid deposition of amorphous carbon deposit on the substrate.

Ni_2Si is formed in most composition range in Ni-SiO_2-CH_4. Silicon is a material that can decrease the catalytic efficiency of the metal and retard the graphitization of carbon. On the other hand, it is observed that the silicide phase is suppressed to form in Ni-SiO_2-CO, which means that the Ni clusters remain unaffected by silicon and active as catalysts and nucleation sites of graphene layers.CO and hydrogen mixed atmosphere can etch solid carbon. High strain energy involved in carbon nanotube tip makes it more vulnerable to the etch environment. It could provide a better situation to keep the tip of carbon nanotube open and chemically active.

Laterally aligned carbon nanotubes were synthesized on substrates over iron nanoparticles by using chemical vapor deposition. In addition, aligned carbon nanotubes grown vertically and with tilt angle to the substrates were produced, which means that it is possible to grow aligned carbon nanotubes at any angle relative to the substrate. The growth direction of the carbon nanotubes was controlled by a magnetic field that is applied in the process of adhering catalyst particles on silicon oxide substrates from dispersion. The ferromagnetic property of the iron nanoparticles fixes them in a defined orientation under magnetic field, which results in aligned growth of the carbon nanotubes. These results indicate that carbon nanotubes preferentially grow from certain facets of the catalyst particles, suggesting a crucial clue in investigating the growth mechanism of carbon nanotubes. The laterally aligned carbon nanotubes could make it possible to integrate them in nano-electronic devices, such as a channel for field effect transistors.

The growth of CNT seems to depend on complicated interaction between the vapor phase and supporting oxides. CH_4 is a stable hydrocarbon source and need a high process temperature for the growth of carbon nanotubes. Therefore, the experiment was carried out in a very limited process temperature. In order to understand the growth mechanism of carbon nanotubes, investigation in wide temperature range is necessary. Usage of a different carbon source, such as acetylene and ethylene, leads to a lower process temperature would give different growth characteristics.

APPENDIX A
FACTSAGE

FactSage[105] is the combined version of FACT-Win and ChemSage designed to facilitate calculations of complex equilibrium in multicomponent, multiphase systems. The program operates under Windows and incorporates all the features offered by these two internationally widely used software, but in an improved and further developed form.

Utilized Code: ChemSage (Gibbs Energy Minimization code, which is the latest version of SolGasMix code)

1. Data Bases

- Compound Databases – note: a compound may contain several phases
  - FACT - F*A*C*T 5.0 compound database (over 4,400 compounds)
  - SGPS - SGTE pure substances database (over 3,400 compounds)
  - SGSL - SGTE intermetallic compounds (for use with SGSL solutions)
- Solution Databases
  - FACT - F*A*C*T 5.0 solution database (120 non-ideal multicomponent phases)
  - SGSL - SGTE alloy solutions database (63 non-ideal multicomponent alloy and carbonitride phases)

2. FactSage Thermodynamic Models (Calculational Modules of FactSage)

2.1. Stoichiometric Reactions

This approach is applied to Reaction module of FactSage.

Equilibrium $\rightarrow$ G(Gibbs free energy) = minimum or $\Delta G = 0$

Consider the reation: $\upsilon_A A + \upsilon_B B + ... = \upsilon_S S + \upsilon_T T + \ldots$

For constant T(temperature) and p(pressure), i.e. dT = 0 dp = 0

$$dG = \sum_i \mu_i dn_i$$

For a stoichiometric reaction, the changes dni are given by the stoichiometric coefficients υi and change in extend of reaction $d\zeta$.

$$dn = \upsilon_i d\zeta$$

Thus the problem becomes one-dimensional.

$$dG = \sum_i \mu_i \upsilon_i d\zeta = 0$$

Separation of variable:

$$dG/\, d\zeta = \sum_i \mu_i \upsilon_i = 0$$

Thus the equilibrium condition for a stoichiometric reaction:

$$\Delta G = \sum_i \mu_i \upsilon_i = 0$$

Introduction of standard potential μ_i^0 and activites a_i yields:

$$\mu_i = \mu_i^0 + RT\ln a_i$$

$$\sum_i \upsilon_i \mu_i^0 + RT \sum \upsilon_i (\ln a_i) = 0$$

It follows the law of Mass Reaction:

$$\Delta G^0 = \sum_i \upsilon_i \mu_i^0 = -RT\ln \prod a_i^{\upsilon i}$$

Here, $K = \prod a_i^{\upsilon i}$ is the well-known Equilibrium Constant.

The reaction module in FactSage permits a multitude of calculations which are based on the law of Mass Action. The reaction module calculates changes in extensive thermochemical properties (H,G,V,S,Cp,A) for a single species, a mixture of species or for a chemical reaction. The species may be pure elements, stoichimetric compounds or ions(both plasma and aqueous ions).

2.2. Multi Component Multi Phase Approach

This approach is applied to Equilibrium module of FactSage.

Complex equilibria: Many components, many phases(solution phases)

Assuming constant T and p

$$G = \min$$

with $$G = \sum_i n_i \mu_i = \sum_i n_i(\mu_i + \mathrm{RT ln} a_i)$$

or $$G = \sum_{\varphi} \{ \sum_{i}^{m_\varphi} n_i^{\varphi} \} G_m^{\varphi}$$

Here, G_m^{φ} is the molar integral Gibbs energy of phase φ and n_i^{φ} are the mole numbers of the phase constituents *i* of the phase

Massbalance constraint:

$$\sum_j a_{ij} n_i = b_j$$

are subsidiary conditions. n_i is the mole number of species *i*, a_{ij} are the stoichiometric coefficients of species *i*, with respect to the components of the system ($j = 1$ to m), and b_j is the total amount of component *j*.

Lagrangeian multipliers M_j turn out to be the chemical potentials of the system components at equilibrium

$$G = \sum_j b_j M_j$$

Modelling of Gibbs energy of phases

$$G_m^{\varphi} = G_m^{\varphi}(T, n_i^{\varphi}, p)$$

Pure substance (stoichiometric): $G_m^{\varphi} = \mu_i^{0,\varphi} = G^{0,\varphi}(T, p)$

Solution phase: $G_m^{\varphi} = G_m^{\varphi,ref} + G_m^{\varphi,id} (= -T\Delta S_m^{id}) + G_m^{\varphi,ex}$

The first term contains the contribution of the pure phase constituents, the second term gives the contribution due to the ideal mixing of the chosen phase constituents, and

the third term contains non-ideal (excess) contributions with respect to the chosen ideal mixing.

Use of the equilibrium module to execute a multitude of calculations based on the complex equilibrium approach outlined above. The equilibrium module is the Gibbs energy minimization workshore of FactSage. It calculates the concentrations of chemical species when specified elements or compounds react or partially react to reach a state of chemical equilibrium. The equilibrium module employs the Gibbs energy minimization algorithm and thermochemical functions of ChemSage and offers great flexibility in the way the calculations may be performed.

2.3. How the phase diagram module works

Phase diagram is a generalized module that permits one to calculate, plot and edit unary, binary, ternary and multicomponent phase diagram sections where the axes can be various combinations of T,P,V, composition, activity, chemical potential, etc. The resulting phase diagram is automatically plotted by the Figure module. The possible types of phase diagram sections that may be calculated are based on a thermodynamically consistent theory of generalized phase diagram mapping. Similar to the rules outlined by Hillert[106] a set of simple rules has been derived that dictate what axes and constants constitute a true phase diagram. The Zero Phase Fraction (ZPF) line principles was introduced by Morral and co-workers[107-109] All true two-dimensional sections consist of a collection of ZPF lines, one for each phase. The phase appears on one side of its ZPF lines and does not appear on the other, and the ZPF line either forms a closed loop inside the diagram or terminates at the edges of the diagram. In FactSage this has been combined with the phase diagram rules in order to derive a strategy for the mapping of a

complete phase diagram without the need for user-defined starting points. This greatly simplifies the strategy for mapping the complete phase diagram since it is simply a question of tracing all ZPF lines.

APPENDIX B
THERMODYNAMIC DATA CALCULATED BY FACTSAGE

The data are calculated by the equilibrium module of FactSage. It is assumed that equilibrium is established during the process and that the gases behave ideally and gas and solid phases are present in the system. The input is temperature, pressure, reaction components, the amount of the each component (composition). The output is chemical components which exist in the system when the system reaches to the equilibrium state, the amount of the components present and their mole fractions.

1. Chemical gas components generated from oxide powder in CH_4-H_2 flow system at the process temperature

In this calculation, the input is1050°C (temperature), 1atm (pressure), reaction components (assume 1 mole of oxide, 1 mol of H_2, 0.05 mol of CH_4).

1.1 SiO_2

```
T = 1050.00 C
P = 1.00000E+00 atm
V = 1.19338E+02 dm3

STREAM CONSTITUENTS          AMOUNT/mol
SiO2_quartz(1)(s)_FACT       1.0000E+00
CH4_FACT/gas_ideal/          5.0000E-02
H2_ELEM/gas_ideal/           1.0000E+00

                             EQUIL AMOUNT   MOLE FRACTION
PHASE: gas_ideal               mol
H2_FACT                      5.4816E-01     4.9872E-01
H2_ELEM                      5.4816E-01     4.9872E-01
CH4_FACT                     1.8347E-03     1.6692E-03
CO_FACT                      9.6685E-04     8.7965E-04
H2O_FACT                     3.5924E-06     3.2684E-06
H_FACT                       1.2266E-06     1.1159E-06
SIO_FACT                     8.1753E-07     7.4380E-07
C2H2_FACT                    5.3126E-07     4.8334E-07
C2H4_FACT                    4.9313E-07     4.4865E-07
CH3_FACT                     9.6568E-08     8.7858E-08
TOTAL:                       1.0991E+00     1.0000E+00
```

1.2 $SiO_2/Fe(NO_3)_3$

T = 1050.00 C
P = 1.00000E+00 atm
V = 1.19774E+02 dm3

STREAM CONSTITUENTS	AMOUNT/mol
CH4_FACT/gas_ideal/	5.0000E-02
H2_ELEM/gas_ideal/	1.0000E+00
SiO2_quartz(l)(s)_FACT	1.0000E+00
Fe_bcc(s)_ELEM	3.0000E-03

PHASE: gas_ideal	EQUIL AMOUNT mol	MOLE FRACTION
H2_FACT	5.4816E-01	4.9691E-01
H2_ELEM	5.4816E-01	4.9691E-01
CO_FACT	4.9757E-03	4.5104E-03
CH4_FACT	1.8280E-03	1.6571E-03
H2O_FACT	1.8420E-05	1.6698E-05
H_FACT	1.2288E-06	1.1139E-06
C2H2_FACT	5.3126E-07	4.8158E-07
C2H4_FACT	4.9133E-07	4.4539E-07
SiO_FACT	1.6002E-07	1.4506E-07
CH3_FACT	9.6392E-08	8.7379E-08
CO2_FACT	9.1421E-08	8.2873E-08
TOTAL:	1.1031E+00	1.0000E+00

1.3 TiO_2

T = 1050.00 C
P = 1.00000E+00 atm
V = 1.24848E+02 dm3

STREAM CONSTITUENTS	AMOUNT/mol
TiO2_rutile(s)_FACT	1.0000E+00
CH4_FACT/gas_ideal/	5.0000E-02
H2_ELEM/gas_ideal/	1.0000E+00

PHASE: gas_ideal	EQUIL AMOUNT mol	MOLE FRACTION
H2_FACT	5.4741E-01	4.7606E-01
H2_ELEM	5.4741E-01	4.7606E-01
CO_FACT	4.9688E-02	4.3212E-02
H2O_FACT	5.0491E-03	4.3910E-03
CO2_FACT	2.5059E-04	2.1793E-04
CH4_FACT	6.1044E-05	5.3088E-05
H_FACT	1.2537E-06	1.0903E-06
H2CO_FACT	2.2596E-08	1.9651E-08
TOTAL:	1.1499E+00	1.0000E+00

2. Calculated Thermodynamic Data in CO-H_2-C System

In this calculation, the input is 1050°C, 1 atm, reaction components (assume that 1 mol of CO, 1 mol of carbon (graphite) and H_2, ranging 0.5 to 20 mol, are present in the system). The data is shown for 0.5 mol of H_2, and 20 mol of H_2.

T = 1323.00 K
P = 1.00000E+00 atm
V = 1.62166E+02 dm3

STREAM CONSTITUENTS	AMOUNT/mol
CO/gaa_idaal/	1.0000E+00
H2/gas_ideal/	5.0000E-01
C_graphita(a)	1.0000E+00

PHASE: gas_idaal		EQUIL AMOUNT mol	MOLE FRACTION	FUGACITY atm
CO		9.9217E-01	6.6421E-01	6.6421E-01
H2		4.9534E-01	3.3161E-01	3.3161E-01
CO2		2.6892E-03	1.8003E-03	1.8003E-03
H2O		2.4546E-03	1.6432E-03	1.6432E-03
CH4		1.1034E-03	7.3867E-04	7.3867E-04
H		1.3561E-06	9.0786E-07	9.0786E-07
C2H2		4.7896E-07	3.2064E-07	3.2064E-07
H2CO		3.1432E-07	2.1043E-07	2.1043E-07
C2H4		2.9618E-07	1.9828E-07	1.9828E-07
CH3		7.1056E-08	4.7569E-08	4.7569E-08
CH2CO	T	1.6096E-08	1.0775E-08	1.0775E-08
HCO		3.0102E-09	2.0152E-09	2.0152E-09
C2H6	T	3.7685E-10	2.5228E-10	2.5228E-10
CH3OH	T	1.0201E-10	6.8294E-11	6.8294E-11
OH		1.0016E-10	6.7055E-11	6.7055E-11
HCOOH		1.4330E-11	9.5931E-12	9.5931E-12
C2H3		7.8213E-12	5.2360E-12	5.2360E-12
C3O2		3.0977E-12	2.0738E-12	2.0738E-12
C2H4O(g2)	T	2.0041E-12	1.3417E-12	1.3417E-12
C2H		7.6895E-13	5.1478E-13	5.1478E-13
CH2		1.7168E-13	1.1494E-13	1.1494E-13
C2O		1.0704E-14	7.1658E-15	7.1658E-15
CH3CH2OH(g)		6.8236E-15	4.5681E-15	4.5681E-15
CH3COOH	T	5.0014E-15	3.3482E-15	3.3482E-15
O		2.5134E-16	1.6826E-16	1.6826E-16
C2H4O(g)		1.5996E-16	1.0708E-16	1.0708E-16
CH		2.1864E-18	1.4637E-18	1.4637E-18
O2		6.0485E-19	4.0492E-19	4.0492E-19
CH3CH2OH(g2)	T	5.2489E-19	3.5139E-19	3.5139E-19
HOOH		1.0153E-19	6.7971E-20	6.7971E-20
C		1.1532E-20	7.7203E-21	7.7203E-21
C3		1.2564E-21	8.4112E-22	8.4112E-22
HOO		1.2026E-21	8.0506E-22	8.0506E-22
C2		1.6917E-23	1.1325E-23	1.1325E-23
C5		7.2772E-28	4.8718E-28	4.8718E-28
C4		5.2859E-28	3.5387E-28	3.5387E-28
O3		2.2998E-37	1.5396E-37	1.5396E-37
TOTAL:		1.4938E+00	1.0000E+00	1.0000E+00
		mol		ACTIVITY
C_graphita(a)		1.0040E+00		1.0000E+00
C_diamond(s2)		0.0000E+00		5.1446E-01
H2O_ica(s)	T	0.0000E+00		5.0695E-09

Cp_EQUIL J.K-1	H_EQUIL J	H_EQUIL J.K-1	G_EQUIL J	V_EQUIL dm3
7.75485E+01	-4.43535E+04	3.69364E+02	-5.33023E+05	1.62166E+02

Mola fraction of ayatem componants:

	gaa_idaal
O	3.3378E-01
C	3.3243E-01
H	3.3378E-01

Data on 7 constituents markad with 'T' ars extrapolated outaida thsir valid tamparatura ranga

T = 1323.00 K
P = 1.00000E+00 atm
V = 2.26541E+03 dm3

STREAM CONSTITUENTS	AMOUNT/mol
CO/gaa_ideal/	1.0000E+00
H2/gas_idaal/	2.0000E+01
C_graphits(s)	1.0000E+00

PHASE: gas_ideal		EQUIL AMOUNT mol	MOLE FRACTION	FUGACITY atm
H2		1.9742E+01	9.4607E-01	9.4607E-01
CO		9.9261E-01	4.7568E-02	4.7568E-02
CH4		1.2547E-01	6.0125E-03	6.0125E-03
H2O		7.0061E-03	3.3574E-04	3.3574E-04
CO2		1.9267E-04	9.2331E-06	9.2331E-06
C2H4		3.3678E-05	1.6139E-06	1.6139E-06
H		3.1999E-05	1.5335E-06	1.5335E-06
C2H2		1.9089E-05	9.1480E-07	9.1480E-07
CH3		4.7834E-06	2.2923E-07	2.2923E-07
H2CO		8.9717E-07	4.2994E-08	4.2994E-08
C2H6	T	1.2225E-07	5.8586E-09	5.8586E-09
CH2CO	T	4.5942E-08	2.2016E-09	2.2016E-09
HCO		5.0868E-09	2.4377E-10	2.4377E-10
CH3OH	T	8.3073E-10	3.9810E-11	3.9810E-1I
C2H3		5.2653E-10	2.5232E-11	2.5232E-11
OH		1.6926E-10	8.1113E-12	8.1113E-12
C2H		1.8144E-11	8.6950E-13	8.6950E-13
C2H4O(g2)	T	1.6320E-11	7.8209E-13	7.8209E-13
CH2		6.8426E-12	3.2791E-13	3.2791E-13
HCOOH		2.9291E-12	1.4037E-13	1.4037E-13
C3O2		2.2194E-13	1.0636E-14	1.0636E-14
CH3CH2OH(g)		1.5853E-13	7.5970E-15	7.5970E-15
C2O		1.0709E-14	5.1318E-16	5.1318E-16
CH3COO8	T	2.9167E-15	1.3977E-16	1.3977E-16
C2H4O(g)		1.3026E-15	6.2421E-17	6.2421E-17
O		2.5145E-16	1.2050E-17	1.2050E-17
CH		5.1591E-17	2.4723E-18	2.4723E-18
CH3CH2OH(g2)	T	1.2195E-17	5.8439E-19	5.8439E-19
C		1.6110E-19	7.7203E-21	7.7203E-21
O2		4.3335E-20	2.0767E-21	2.0767E-21
HOOH		2.0754E-20	9.9456E-22	9.9456E-22
C3		1.7552E-20	8.4112E-22	8.4112E-22
C2		2.3632E-22	1.1325E-23	1.1325E-23
HOO		1.4553E-22	6.9741E-24	6.9741E-24
C5		1.0166E-26	4.8718E-28	4.8718E-28
C4		7.3843E-27	3.5387E-28	3.5387E-28
O3		1.1800E-39	5.6549E-41	5.6549E-41
TOTAL:		2.0867E+01	1.0000E+00	1.0000E+00
		mol		ACTIVITY
C_graphita(s)		8.8162E-01		1.0000E+00
C_diamond(a2)		0.0000E+00		5.1446E-01
H2O_ics(s)	T	0.0000E+00		1.0358E-09

Cp_EQUIL J.H-1	H_EQUIL J	H_EQUIL J.H-1	G_EQUIL J	V_EQUIL dm3
7.12373E+02	5.41507E+05	3.79436E+03	-4.47843E+06	2.26541E+03

Mols fraction of system componants:

	gas_ideal
O	2.3743E-02
C	2.6553E-02
H	9.4970E-01

Data on 7 constituents marked with 'T' ara axtrapolatad outaida thair valid tempsratura rangs

LIST OF REFERENCES

1. S. Iijima, Nature 354, 56(1991)
2. S. Iijima, T. Ichiahshi, Nature 363, 603(1993)
3. G. G. Tibbetts, J Crystal Growth 66, 632(1984)
4. A. Krishnan, E. Dujardin, T. W. Ebbesen, P. N. Yanilos, M. M. J. Treacy, Phys. Rev. B 58 14013(1998)
5. A. G. Rinzler, J. H. Hafner, P. Nikolaev, L. Lou, S. G. Kim, D. Tomanek, P. Nordlander, D. T. Colbert, R. E. Smalley, Science 269, 1550(1995)
6. L. Chico, V. H. Crespi, L. X. Benedict, S. G. Louie, M. L. Cohen, Phys. Rev. Lett. 76, 971(1996)
7. R. Martel, T. Schmidt, H. R. Shea, T. Hertel, Ph. Avouris, Appl. Phys. Lett. 73, 2447(1998)
8. M. Ouyang, J. –L. Huang, C.L. Cheung, C.M. Lieber, Science 292, 702(2001)
9. P.G. Collins, M.S. Arnold, P. Avouis, Science 292, 706(2001)
10. S.J. Tan, A. R. M. Vershueren, C. Dekker, Nature 393, 49(1998)
11. S. Fan, M. G. Chapline, N. R. Franklin, T. W. Tombler, A. M. Cassell, H. Dai, Science 283,512(1999)
12. J. H. Wang, P. Bush, M. P. Siegal, P. N. Provencio, Science 282, 1105(1998)
13. J. Kong, H. T. Soh, A. M. Cassell, C. F. Quate, H. Dai, Nature 395, 878(1998)
14. A. M. Casell, N. R. Franklin, T. W. Tombler, E. M. Chan, J. Han, H. Dai, J. Am. Chem. Soc. 121, 7975(1999)
15. Y.-S. Han, J.-K. Shin, S.-T. Kim, J. Appl. Phys. 90, 5731(2001)
16. H. Dai, J. Kong, C. Zhou, N. Franklin, T. Tombler, A. Cassell, S. Fan, M. Chapline, J. Phys. Chem. 103, 11246(1999)
17. V. I. Merkulov, D. H. Lowndes, Y. Y. Wei, G. Eres, and E. Voekl, Appl. Phys. Lett. 76, 3555(2000)

18. R.T.K.Baker, Carbon 27, 315(1989)

19. K. B. K. Teo, M. Chhowalls, G. A. J. Amartuga, and W. I. Milne, Appl. Phys. Lett. 79, 1534(2001)

20. Y. Saito, T. Yoshikawa, S. Bandow, M. Tomita, T. Hayashi, Phys. Rev. B 48, 1907(1997)

21. M. Endo, K. Takeuchi, T. Hiraoka, T. Furuta, T. Kasai, X. Sun, C.H. Kiang, M.S. Dresselhaus, J. Phys. Chem. Solids 58, 1707(1997)

22. C.H. Kiang, M. Endo, P.M. Ajayan, G. Dresselhaus, M.S. Dresselhaus, Phys. Rev. Rett. 81. 1869(1998)

23. A. Bachtold, C. Strunk, J.P. Salvetat, J.M. Bonard, L. Forro, T. Nussbaumer, C. Schonenberger, Nature 397, 673(1999)

24. M.S. Dresselhaus, G. Desselhaus, R. Saito, Carbon 33, 883(1995)

25. J.W. Mintmire, C.T. White, Carbon 33, 893(1995)

26. T.W. Odom, J.L. Huang, P. Kim, C.M. Lieber, Nature 391, 62(1998)

27. J.W.G. Wildoer, L.C. Venema, A.G. Rinzler, R.E. Smalley, C. Dekker, Nature 391, 59(1998)

28. R.T.K. Baker, P. S. Harris, R. B. Thomas, R. J. Waite, J. Catal. 30, 86(1994)

29. R.T.K. Baker, N.M. Rodriguez, Mater. Res. Soc. Symp. Proc. 349, 251(1994)

30. J.L. Figueiredo, C.A. Bernardo, J.J. Chludzinski Jr, R.T.K. Baker, J. Catal, 30, 86(1973)

31. A. Oberlin, M. Endo, T. Koyama, J. Cryst. Growth 32, 335(1976)

32. T.W. Ebbesen, Carbon nanotubes, CRC Press Inc, Boca Raton, Florida, 182(1997)

33. A.A. Lucas, P.H. Lamblin, R.E. Smalley, J. Chem. Phys. Solids 54, 587(1993)

34. M.S. Dresselhaus, G. Desselhaus, R. Saito, Phys. Rev. B 45, 6234(1992)

35. H. Kind, J.-M. Bonard, Ch. Emmenegger, L.O. Nilsson, K. Hernadi, E. Mailard-Schaller, L. Schlapach, L. Forro, K. Kern, Adv. Mater. 11, 1285(1999)

36. C.J. Lee, J. Park, S.Y. Kang, J.H. Lee, Chem. Phys. Lett. 323, 554(2000)

37. J. Kong, H.T. Soh, A. M. Cassell, C.F. Quate, H. Dai, Nature 395, 878(1998)

38. A.M. Cassel, J.A. Raymakers, J. Kong, H. Dai, J. Phys. Chem. B 103, 6484(1999)

39. M. Su, B. Zheng, J. Liu, Chem. Phys. Lett. 322, 321(2000)

40. J.H. Hafner, M.J. Bronikowski, B.R. Azamian, P. Nikolaev, A.G. Rinzler, D.T. Colbert, K.A. Smith, R.E. Smalley, Chem. Phys. Lett. 296, 195(1998)

41. K. Hernadi, A. Fonseca, J.B. Nagy, D. Bernaerts, A.A. Lucas, Carbon 34, 1249(1999)

42. A. Peigney, Ch. Laurent, A. Rousset, J. Mater. Chem. 9, 1167(1999)

43. H. Dai, A.G. Rinzler, P. Nikolaev, A. Thess, D.T. Colbert, R.E. Smalley, Chem. Phys. Lett. 260, 471(1996)

44. P. Nikolaev, Michael, J. Bronikowski, R. Kelley Bradley, F. Rohmund, D.T. Colbert, K.A. Smith, R.E. Smalley, Chem. Phys. Lett. 313, 91(1999)

45. C. Bower, W. Zhu, S. Jin. O. Zhou, Appl. Phys. Lett. 77, 830(2000)

46. V.I. Merkulov, D.H. Lowndes, Y.Y. Wei, G. Eres, E. Voelkl, Appl. Phys. Lett. 76, 3555(2000)

47. K.B.K. Teo, M. Chhowalla, G.A. Amaratunga, W.I. Milne, D.G. Hasko, G. Pirio, P. Legagneux, F. Wyczisk, D. Pribat, Appl. Phys. Lett. 79, 1534(2001)

48. L. Delzeit, I. McAninch, B.A. Cruden, D. Hash, B. Chen, J. Han, M. Meyyappan, J. Appl. Phys. 91, 6027(2002)

49. Z.F Ren, Z.P. Huang, J.W. Xu, J.H. Wang, P. Bush, M.P. Siegel, P.N. Provencio, Science 282, 1105(1998)

50. C. Bower, W. Zhu, S.H. Jin, O. Zhou, Appl. Phys. Lett. 77, 830(2000)

51. S.H. Tsai, C.W. Chao, C.L. Lee, H.C. Shih, Appl. Phys. Lett. 74, 3462(2000)

52. M. Chhowalla, K.B.K. Teo, C. Ducati, N.L. Rupesinghe, G.A.J. Amaratuga, A.C. Ferrari, D. Roy, J. Robertson, W.I. Milne, J. Appl. Phys. 90, 5308(2001)

53. J.I. Sohn, S. Lee, Y.H. Song, S.Y. Choi, K.I. Cho, K.S. Nam, Appl. Phys. Lett. 78, 901(2001)

54. T. de los Arcos, F. Vonau, M.G. Garnier, V. Thommen, H.-G. Boyen, P. Oelhafen, M. Düggelin, D. Mathis, R. Guggenheim, Appl. Phys. Lett. 80, 2383(2002)

55. A.M. Rao, D. Jacques, R.C. Haddon, W. Zhu, C. Bower, S. Jin, Appl. Phys. Lett. 76, 3813(2000)

56. O.A. Nerushev, M. Sveningsson, L.K.L. Falk, F. Rohmund, J. Mater. Chem. 11, 1122(2001)

57. Y. Gao, J. Liu, M. Shi, S.H. Elder, J.W. Virden, Appl. Phys. Lett. 74, 3642(1999)

58. H. Kind, J.M. Bonard, C. Emmenegger, L.O. Nilsson, K. Hernadi, E. Maillard-Schaller, L. Schlapbach, L. Forro, K. Kern, Adv. Mater. 11, 74(1982)

59. A. Fonseca, K. Hernadi, J.B. Nagy, D. Bernaerts, A.A. Lucas, J. Mol. Catal. A: Chemical 107, 159(1996)

60. C. Emmernegger, P. Mauron, A. Zuttel, C. Nutzenadel, A. Schneuwly, R. Gallay, L. Schlapbach, Appl. Surf. Sci. 162, 452(2000)

61. H. Kind, J.M. Bonard, C. Emmenegger, L.O. Nilsson, K. Hernadi, E. Maillard-Shcaller, L. Schlapbach, L. Forro, K. Kern, Adv. Mater. 11, 1285(1999)

62. Y.Y. Wei, G. Eres, V.I. Merkulov, D.H. Lowndes, Appl. Phys. Lett. 78, 1394(2001)

63. M.P. Siegal, D.L. Overmyer, P.P. Provencio, Appl. Phys. Lett. 80, 2171(2002)

64. C. Ducati, I. Alexandrou, M. Chhowalla, G.A. Amaratunga, J. Robertson, J. Appl. Phys. 92, 3299(2002)

65. Z.W. Pan, S.S. Xie, B.H. Chang, C.Y. Wang, L. Lu, W. Liu, M.Y. Zhou, W.Z. Li, Nature 394, 631(1998)

66. T. Kyotani, L.F. Tsai, A. Tomita, Chem. Mater. 7, 1427(1995)

67. J. Li, C. Papadopoulos, J.M. Xu, M. Moskovits, Appl. Phys. Lett. 75, 367(1999)

68. J. Kong, H. T. Soh, A. M. Cassell, C. F. Quate, H. Dai, Nature 395, 878(1998)

69. A. M. Casell, N. R. Franklin, T. W. Tombler, E. M. Chan, J. Han, H. Dai, J. Am. Chem. Soc. 121, 7975(1999)

70. Y.G. Zhang, A.L. Chang, J. Cao, Q. Wang, W. Kim, Y.M. Li, N. Morris, E. Yenilmez, J. Kong, H. Dai, Appl. Phys. Lett. 79, 3155(2001)

71. A. Ural, Y. Li, H. Dai, Appl. Phys. Lett. 81, 3464(2002)

72. S. Iijima, J. Crystal Growth 50, 675(1980)

73. T.W. Ebbesen, P.M. Ajayan, Nature 358, 220(1992)

74. W. A. de Heer, D. Ugarte, Chem. Phys. Lett. 207, 480 (1993)

75. D. Ugarte, Chem. Phys. Lett 207, 473(1993)

76. V. L. Kuznetsov, A. L. Chuvilin, Yu. V. Butenko, I. Yu. Malkov, V. M. Titov, Chem. Phys. Lett. 222, 343(1994)

77. T. Gorelik, S. Urban, F. Falk, U. Kaiser, U. Glatzel, Chem. Phys. Lett. 373, 642(2003)

78. S Tomita, T. Sakurai, H. Ohta, M. Fujii, S. Hayashi, J. Chem. Phys. 114, 7477(2001)

79. D. Ugarte, Nature 359, 707(1992)

80. D. Ugarte, Europhys. Lett. 22, 45(1993)

81. D. Ugarte, Carbon 33, 989(1995)

82. E. D. Obraztosova, M. Fujii, S. Hayashi, V. L. Kuznetsov, Y. V. Butenko, A. L. Chuvilin, Carbon 36, 821(1998)

83. S. Tomita, M. Fujii, S. Hayashi, K. Yamamoto, Chem. Phys. Lett. 305, 225(1999)

84. Y. Saito, T. Yoshikawa, J. Cryst. Growth 134, 154(1993)

85. Y. Saito, Carbon 33, 979(1995)

86. Y.F. Li, J.S. Qiu, Z.B. Zhao, T.H. Wang, Y.P. Wang, W. Li, Chem. Phys. Lett. 366, 544(2022)

87. V. V. Kovalevski, A. N. Safronov, Carbon 36, 963(1998)

88. C.J. Lee, J. Park, Appl. Phys. Lett. 77, 3397(2000)

89. R. Andrews, D. Jacques, A. M. Rao, F. Derbyshire, D. Qian, X. Fan, E. C. Dickey, J. Chen, Chem. Phys. Lett. 303, 467(1999)

90. H. Cui, O Zhou, B. R. Stoner, J. Appl. Phys. 88, 6072(2000)

91. Y.H. Lee, Y.T. Jang, C.H. Choi, D.H. Kim, C.W. Lee, J.E. Lee, Y.S. Han, S.S. Yoon, J.K. Shin, S.T. Kim, E.K. Kim, B.K. Ju, Adv. Mater. 13, 1371(2001)

92. J. W. Ward, B. Q. Wei, P. M. Ajayan, Chem. Phys. Lett. 376, 717(2003)

93. Y. Murakami, Y. Miyauchi, S. Chiashi, S. Maruyama, Chem. Phys. Lett. 377, 49(2003)

94. S. Iijima, P.M. Ajayan, T. Ichihashi, Phys. Rev. Lett. 69, 3100(1992)

95. A. Fissel, B. Schroter, W. Richter, Appl. Phys. Lett. 66, 3182(1995)

96. H. Dai, E. W. Wong, Y. Z. Lu, S. Fan, C. M. Lieber, Nature 375, 769(1995)

97. G. W. Meng, Z. Cui, L. D. Zhang, F. Philipp, J. Cryst. Growth 209, 801(2000)

98. Q. Lu, J. Hu, K. Tang, Y. Qian, G. Zhou, X. Liu, J. Zhu, Appl. Phys. Lett. 75, 507(1999)

99. C. H. Liang, G. W. Meng, L. D. Zhang, Y. C. Wu, Z. Cui, Chem. Phys. Lett. 329, 323(2000)

100. H. Y. Peng, X. T. Zhou, H. L. Lai, N. Wang, S. T. Lee, J. Mater. Res. 15, 2020 (2000)

101. Y. B. Li, S. S. Xie, X. P. Zou, D. S. Tang, Z. Q. Liu, W. Y. Zhou, G. Wang, J. Cryst. Growth 223, 125(2001)

102. J. C. Li, C. S. Lee, S. T. Lee, Chem. Phys. Lett. 355, 147(2002)

103. S. Iijima, J. Cryst. Growth 50, 675 (1980)

104. S. -J. Park, S Kim, S Lee, Z. G. Khim, K. Char, T. Hyeon, J. Am. Chem. Soc. 122, 8581(2000)

105. C.W. Bale, P. Chartrand, S.A. Degterov, G. Eriksson, K. Hack, R.B. Mahfoud, J. Melancon, A.D. Pelton, S. Petersen, Calphad 26, 189(2002)

106. M. Hillert, J. Phase Equilibria 18(3), 249(1997)

107. T.R. Bramblett, J.E. Morral, Bull. Alloy Phase Diagrams 5, 433(1984)

108. J.E. Morral, Scripta Metallurgica 18, 407(1984)

109. H. Gupta, J.E. Morral, H. Nowontny, Scripta Metall. 20, 889(1986)

BIOGRAPHICAL SKETCH

Ki-Hong Lee was born in Jeju-do, Republic of Korea. He entered the Department of Ceramic Engineering at Yonsei University in 1988. After earning a Bachelor of Science degree at the university, he joined Korea Advanced Institute of Science and Technology (KAIST) in the Ceramic Science and Engineering Department in 1992. He earned a Master of Science degree in 1994. His research topic for the master degree was the pyroelectric properties and phase transition properties of ferroelectric materials. After graduating in 1994, he worked for Samung Electronics, Co., Ltd. until 1998. He was in the field of semiconductor process development, and involved in several research projects, regarding a titanium metal gate for DRAM devices, nonvolatile ferroelectric memory devices, aluminum metallization and SOI (Silicon On Insulator) devices. In 1998, he joined the Atomic-scale Surface Science Research Center at Yonsei University. In 2000, he was admitted to the Department of Materials Science and Engineering at the University of Florida to pursue Ph.D. degree. His research field in Dr. Sigmund's group was the growth of carbon nanotubes and semiconductor nanowire on silicon using the chemical vapor deposition method. In particular, the research was focused on the growth mechanism of nanotubes and controlling their growth direction for future application to nano electrical, optical, and biological devices. He obtained his Ph.D. degree in May 2004.

I certify that I have read this study and that in my opinion it conforms to acceptable standards of scholarly presentation and is fully adequate, in scope and quality, as a dissertation for the degree of Doctor of Philosophy.

Wolfgang M. Sigmund, Chair
Associate Professor of Materials Science and Engineering

I certify that I have read this study and that in my opinion it conforms to acceptable standards of scholarly presentation and is fully adequate, in scope and quality, as a dissertation for the degree of Doctor of Philosophy.

David P. Norton
Professor of Materials Science and Engineering

I certify that I have read this study and that in my opinion it conforms to acceptable standards of scholarly presentation and is fully adequate, in scope and quality, as a dissertation for the degree of Doctor of Philosophy.

Rajiv K. Singh
Professor of Materials Science and Engineering

I certify that I have read this study and that in my opinion it conforms to acceptable standards of scholarly presentation and is fully adequate, in scope and quality, as a dissertation for the degree of Doctor of Philosophy.

Susan Sinnott
Associate Professor of Materials Science and Engineering

I certify that I have read this study and that in my opinion it conforms to acceptable standards of scholarly presentation and is fully adequate, in scope and quality, as a dissertation for the degree of Doctor of Philosophy.

Andrew G. Rinzler
Associate Professor of Physics

This dissertation was submitted to the Graduate Faculty of the College of Engineering and to the Graduate School and was accepted as partial fulfillment of the requirements for the degree of Doctor of Philosophy.

May 2004

Pramod P. Khargonekar
Dean, College of Engineering

Kenneth J. Gerhardt
Interim Dean, Graduate School